TRIBHUVAN UNIVERSITY

INSTITUTE OF ENGINEERING

PULCHOWK CAMPUS

B-10-BME-2018/2023

Design And Fluid-Structure Interaction Study of a Wing Structure for a Medium-Range UAV

by

Badal Tamang (075BME013)

Ishan Ghimire (075BME020)

Uttam Bohara (075BME048)

A PROJECT REPORT

SUBMITTED TO THE DEPARTMENT OF MECHANICAL AND AEROSPACE ENGINEERING

IN PARTIAL FULFILLMENT OF THE REQUIREMENT FOR THE

DEGREE OF BACHELOR IN MECHANICAL ENGINEERING

DEPARTMENT OF MECHANICAL AND AEROSPACE ENGINEERING

LALITPUR, NEPAL

APRIL 2023

COPYRIGHT

TRIBHUVAN UNIVERSITY

INSTITUTE OF ENGINEERING

PULCHOWK CAMPUS

DEPARTMENT OF MECHANICAL AND AEROSPACE ENGINEERING

The undersigned certify that they have read, and recommended to the Institute of Engineering for acceptance, a project report entitled "Design and Fluid-Structure Interaction Study of a Wing Structure for a Medium Range UAV" submitted by Badal Tamang, Ishan Ghimire and Uttam Bohara in partial fulfilment of the requirements for the degree of Bachelor of Mechanical Engineering.

_____

Supervisor, Asst. Prof. Neeraj Adhikari

Department of Mechanical and Aerospace Engineering

_____

Supervisor, Asst. Prof. Laxman Motra

Department of Mechanical and Aerospace Engineering

_____

External Examiner, Er. Siddhartha Poudel

Lecturer

Everest Engineering College

_____

Committee Chairperson, Dr. Surya Prasad Adhikari

Head, Department of Mechanical and Aerospace Engineering

IOE Pulchowk Campus

_____

Date

ABSTRACT

This report presents the design of wing structure of a medium-range fixed-wing unmanned aerial vehicle (UAV) to carry a payload of 25 kg, and the Fluid-Structure Interaction (FSI) study of the designed wing for design validity and aerodynamic performance enhancement. FSI simulation helps us to study the performance of aircrafts in an economic and faster way, without having to conduct experiments every time, so that we can easily rectify faults and optimize the design. In this project, we finalized the flight requirements for the UAV and studied the properties of UAVs having similar requirements. Then, using iterative estimation technique, we calculated gross takeoff weight of the aircraft to be 122 kilograms. We selected appropriate wing configurations and used empirical scaling laws to calculate wing dimensions. After comparing characteristics curves of different airfoils in airfoil tools, we selected Wortmann fx-76-mp-140 airfoil for the wing. Using SOLIDWORKS, we generated a 3D CAD model of the wing structure including main spar, aft spar and ribs. We validated the design using XFLR5 and FSI simulation. We obtained lift to drag ratio, deformation and stress on the wing by performing one-way FSI simulation in ANSYS, where we coupled pressure loads from Fluent to Static Structural module. Finally, we performed different simulations by varying dihedral angle, chord length and wingspan. We compared the results to find optimal configuration to maximize the lift to drag ratio (L/D). Using Analysis of Mean (ANOM), we found that dihedral and chord length had no significant impact on lift to drag ratio. However, the lift to drag ratio increased by 4.9% on increasing wingspan from 4.61 meters to 5.11 meters.

Keywords: Wing, Unmanned Aerial Vehicle, Fluid-Structure Interaction, Lift to drag ratio

ACKNOWLEDGEMENT

First and foremost, we would like to express our sincerest gratitude to the Department of Mechanical and Aerospace Engineering, IOE, Pulchowk Campus for not only providing us this opportunity to work on a project, but also providing us with the necessary resources, facilities, and infrastructure for carrying out the project. We are greatly indebted to our supervisors Asst. Prof. Laxman Motra and Asst. Prof. Neeraj Adhikari for their never-ending support, suggestions, constant encouragement, valuable guidance and constructive critique. Our project would not have reached this point without their utmost support, dedication and passion.

We would like to offer our special thanks to our former supervisor Mr. Rupak Chaudhary for his guidance in the initial phase of our project. He enabled us to have clear vision of path we needed to start and continue the research. We acknowledge him for his supporting and motivating nature.

We heartfully thank our family and friends who helped us on every step for providing us with great support, love, encouragement and feedbacks, which greatly helped us to handle the difficulties.

Once again, thank you all for your invaluable time, support and encouragement. This project would not be possible without your contribution.

TABLE OF CONTENTS

LIST OF TABLES

LIST OF FIGURES

LIST OF SYMBOLS

AC	Aerodynamic Center
b	Wing Span
c_l	Coefficient of lift of airfoil
c_d	Coefficient of drag of airfoil
C_{avg}	Average Chord Length
C_L	Coefficient of lift of wing
C_D	Coefficient of drag of wing
CG	Center of Gravity
C_m	Pitching moment
CP	Centre of Pressure
C_r	Root chord
C_t	Tip chord
M	Mach Number
SFC	Specific Fuel Consumption
S_w	Wing surface area
V_{cruise}	Cruise Velocity
V_{stall}	Stall Velocity
W_e	Empty Aircraft Weight
W_f	Fuel Weight
α	Angle of attack
λ	Taper Ratio
η_p	Propeller Efficiency
ρ_a	Density of Air

LIST OF ABBREVIATIONS

AELS	Automated Emergency Landing System
CFD	Computational Fluid Dynamics
DDPG	Deep Deterministic Policy Gradient
FEA	Finite Element Analysis
FEM	Finite Element Method
FSI	Fluid-Structure Interaction
HALE	High Altitude Long Endurance
ICE	Internal Combustion Engine
MALE	Medium Altitude Long Endurance
NIC	National Innovation Centre
RANS	Reynolds Averaged Navier Stokes
RRT	Rapidly Exploring Random Tree
SAR	Spalart-Allmaras Turbulence
UAV	Unmanned Aerial Vehicles
VTOL	Vertical Take-Off and Landing
ANOM	Analysis of Mean

CHAPTER ONE: INTRODUCTION

1.1 Background

UAV is an aircraft which is either remote-controlled or controlled by on-board computer linked with a ground station. UAV system consists of UAV, ground station and remote controller/transmitter. Free of onboard humans and related risks, they were mostly used in military operations during initial days of development. Now, UAVs have found wider field of application in civil, medical, meteorological, agricultural, commercial and several other sectors.

There are four major types of UAV: single rotor, multi-rotor, fixed wing and hybrid vertical–takeoff and landing (VTOL). But they can be further classified into different categories based on their characteristics as listed in table below:

Table 1.1: Classification of UAV

Characteristics	Categories				
Payload weight (kg)	Nano (<0.25)	Micro (0.25-2)	Small (2-25)	Medium (25-150)	Large (>150)
Range (km)	Very close (< 5)	Close (5-50)	Short (50-150)	Medium (150-650)	Large (>650)
Max. altitude (km)	Close (<1.5)	NATO (1.5-3)	Tactical (3-5.5)	MALE (5.5-9)	HALE (>9)

1.1.1. Fixed Wing UAV

Fixed wing UAV, similar to traditional airplane, has rigid wings to provide lift. It only requires energy to move forward and not to hold itself in air, so it is more efficient than rotor type UAVs. It is powered by electric motors or combustion engines. They can cover larger areas and are suitable for long endurance and long-range flights but are expensive to build. The major components of a fixed wing UAV are as follows:

- Airframe: It is the physical structure of UAV consisting of wings, fuselage, tail, and landing gear. It is designed to be lightweight and durable and its shape is optimized to reduce drag.

- Propulsion: It consists of engine or motor that powers the propeller to generate forward thrust and lift on wings, and battery or fuel system that provides energy to the motor or the engine.
- Payload: It can be the cargo to be delivered, camera, sensors or specialized equipment based on the mission.
- Ground Control Station (GCS): This typically includes computer, software and a controller/joystick for operator to control UAV.
- Avionics: It refers to the electronic systems like flight control system, navigation system, sensor and communication system, which allows UAV to fly autonomously.

1.1.2. Wing Structure and parameters

A wing consists of different components that work together to provide lift, stability and control. Some of the main components of a UAV wing are as follows:

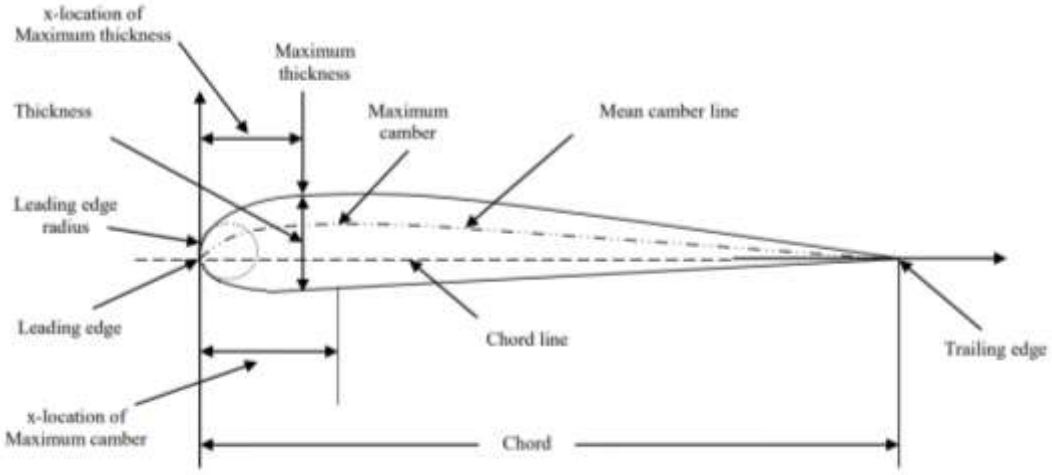

Figure 1.1: Airfoil Geometric Parameters (Sadraey, 2013)

- Airfoil: It is the cross-section shape of a wing that generates aerodynamic lift.
- Wing Spar: It is a beam like structure that runs from wingtip to wing tip. It is the main structural component of the wing.
- Wing Ribs: They are internal structures that give shape to the wing.
- Wing skin: It is outer surface covering of the wing that create wing's aerodynamic shape.
- Wing flaps: These the movable structure at trailing edge of wing that increase the lift of the wing at low speeds.

- Ailerons: These are also the movable section at trailing edge of a wing and are used to control roll of the UAV.
- Winglets: They are small structures at the tip of wing that reduce drag and increase fuel efficiency.

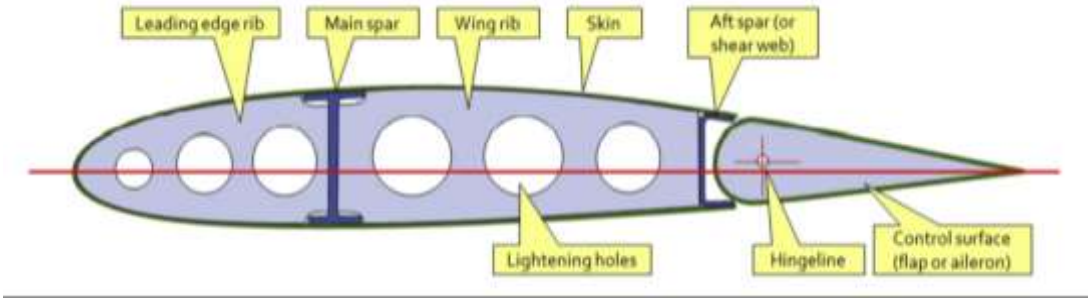

Figure 1.2: Cross- sectional view of wing (Gudmundsson, 2014)

Some of the important wing parameters are as follows:

- Span (b): It is the tip-to-tip distance of awing.
- Chord (c): It is the distance between leading and trailing edge of a wing when measured parallel to the direction of air flow.
- Sweep: It is the certain backward or forward angle of wing made by wing from root to tip. It delays the onset of wave drag and is hence used for high speed aircraft.
- Taper ratio: It is the ratio of tip to root chord lengths of a wing.
- Aspect ratio (AR): It is the ratio of span of a wing to mean aerodynamic chord of the wing. i.e. AR=b/c or AR=b^2/S, where S is wing area.
- Dihedral: It is the upward angle made by wing with the horizontal from root to the tip. It is used to maintain lateral stability of the wing. If the angle is downwards, it is called anhedral.
- Washout: It is the change in wing angle of incidence while moving from root to tip. It ensures that the root stalls before tip so that ailerons can prevent the aircraft from roll.

1.1.3. Fluid-Structure Interaction (FSI) analysis

Fluid structure analysis is one of the numerical simulation techniques which is used to study the behavior of fluid and solid structures when they interact with each other. This technique is used to study various phenomena, like ships' dynamics in rough seas, blood circulation through arteries, and the behavior of aircraft wings in high speed flight. It

basically involves the Computational Fluid Dynamics (CFD) and Finite Element Analysis (FEA) as its basic techniques.

CFD solver simulates the flow of fluid around the solid structure in which fluid solver calculates the pressure, velocity and other properties of the fluid, and provides necessary boundary condition to the FEA solver. Then, FEA solver, in turn, models the behavior of solid structure in terms of deformation and stress distribution.

It is widely used to study wide range of engineering problems and is helping us to understand the complex interactions between fluid and solid components. This makes it possible to optimize the performance of fluid-solid interacting systems in a economical manner.

Fluid-structure interaction simulations involve coupling the fluid flow and structural response of a physical system. The equations that are used to solve FSI problems are derived from the governing equations of fluid dynamics and solid mechanics.

The governing equations for fluid flow analysis in Fluent are the Navier-Stokes equations, which are given by:

$$\rho(\partial u/\partial t + u.\nabla u) = -\nabla p + \nabla.\tau + \rho g \qquad \text{Equation 1.1}$$

where ρ is the density of the fluid, u is the velocity vector, t is time, p is the pressure, τ is the stress tensor, g is the acceleration due to gravity, and ∇ is the gradient operator.

The governing equations for structural analysis in the Static Structural solver are the equations of solid mechanics, which are given by:

$$\nabla.\sigma + f = \rho a \qquad \text{Equation 1.2}$$

where σ is the stress tensor, f is the force vector, ρ is the density of the solid, a is the acceleration, and ∇ is the gradient operator.

To couple the fluid and solid domains, an FSI interface is used. The FSI interface transfers information between the fluid and solid domains, and is based on the interaction of the fluid pressure and the solid deformation.

The equations used to solve the FSI problem are derived from the Navier-Stokes equations and the equations of solid mechanics. The FSI equations can be written as:

$$\rho(\partial u/\partial t + u.\nabla u) = -\nabla p + \nabla.\tau + \rho g$$

$$\nabla.\sigma + f = \rho a$$

$$u = u_s$$

$$\sigma.n - pn = \tau.n \qquad \text{Equation 1.3}$$

where u_s is the solid displacement vector, n is the outward unit normal vector, and pn is the fluid pressure on the solid boundary. These equations describe the coupling between the fluid flow and solid deformation, and are solved iteratively to simulate the FSI behavior of the physical system.

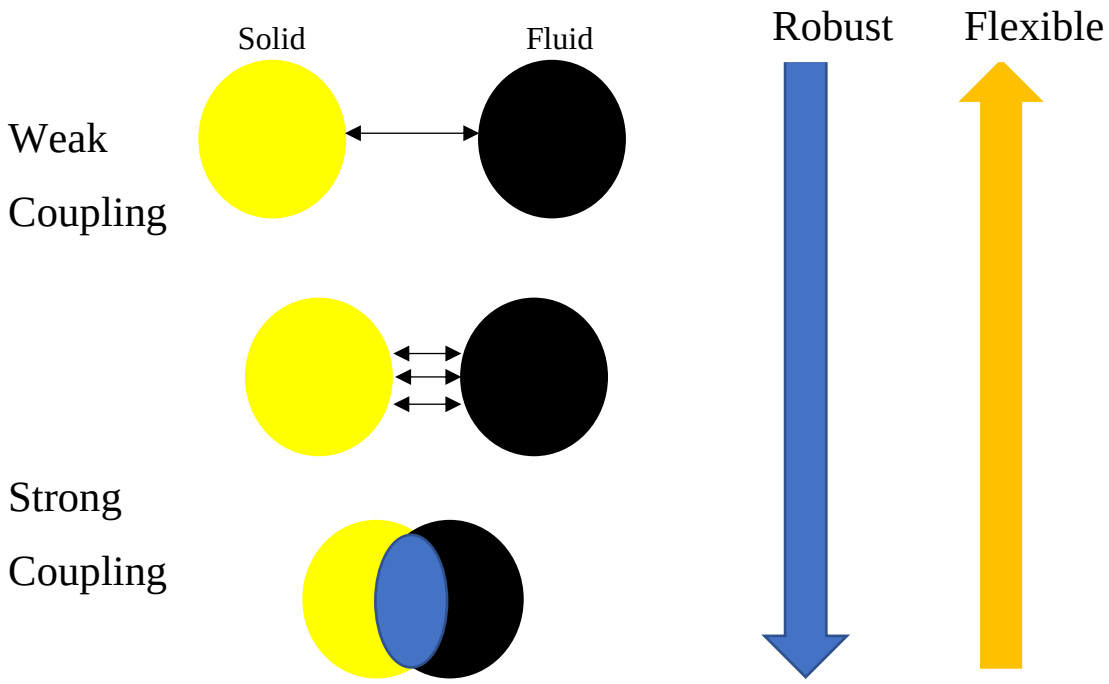

Figure 1.3: Coupling in FSI

In fluid-structure interaction (FSI), the coupling between the fluid and structure can be classified as weak or strong, depending on the level of interaction between the two domains. In weak coupling, the fluid and structure domains are treated as two separate problems that are solved independently. The fluid domain is solved using a CFD solver, while the structure domain is solved using a structural mechanics solver. The interaction between the two domains is considered through boundary conditions or transfer functions. In strong coupling, the fluid and structure domains are solved simultaneously as a fully-coupled problem, where the deformation of the structure affects the fluid flow and vice versa. In weak coupling, the convergence of the solution is typically easier and faster than in strong coupling, as the two domains are solved independently. However,

weak coupling may not accurately capture the dynamic interaction between the fluid and structure domains, leading to potential errors or inaccuracies in the results. Weak coupling is often less computationally expensive than strong coupling, as it requires fewer iterations and computational resources. Overall, the choice between weak and strong coupling in FSI depends on the specific problem and the level of accuracy required. Weak coupling may be suitable for simpler problems or preliminary analysis, while strong coupling is necessary for more complex problems or detailed analysis.

One – way FSI

In this process, hardly fluid domain is affected by the resulting small deformations. It allows the Computational Fluid Dynamics (CFD) and structural analysis to be performed independently with one-way data transfer i.e., from CFD's fluid pressure to structural model. It obtains converged solution from one field and uses it as boundary condition for second field. It is favorable for weak coupling (Ezkurra, et al., 2018).

Two – way FSI

Here, the deformation caused by the fluid pressure affects the flow fluid so fluid and structural domains are solved simultaneously with two-way data transfer. Pressure from CFD is transferred to structural analysis whereas deformation is transferred to fluid domain to update the geometry of fluid domain during every coupling. It is further divided into sub – groups based on degree of coupling as:

- Fully Coupled: It solves both fluid and solid equations in single matrix. Every field remains very tightly coupled in this type; and is very difficult to solve these fluid-structure matrix.
- Iterative Implicit: It solves fluid and structure equations separately. It iterates within each time step to obtain an implicit solution.
- Explicit: Same as implicit except no iteration within a time step. Therefore, it requires much smaller time steps and not recommended.

1.1.4. UAVs in Nepal

Drones are commonly used in Nepal for videography, film-making, surveillance aerial mapping, etc. Most of them are multi-rotor drones. Mahabir Pun's non-profit National Innovation Centre (NIC) developed the country's first "medical drone" in 2018, aiming to bring care to the remote mountain communities that need it most. It can only carry a 1 kg (two pound) load about two 2 km (Sharma G. , 2018). The center is further developing two prototypes, an octocopter and a fixed-wing drone, each with ranges of 15 and 30 km respectively with a maximum load of 3 kg (Shrestha, 2018).

Figure 1.4: Fixed wing drone prototype at NIC (Shrestha, 2018)

(DROTS) Drone Optimized Therapy System, a medical drone made in Nepal recently won the award in the Humanitarian Category along with $5000 at the AUVSI XPONENTIAL AWARDS 2020. These medical drones have been used for six months to deliver samples of around 700 patients for Tuberculosis diagnosis. Furthermore, this scheme assists the Ministry of Health and Population (MoHP) and the National Tuberculosis Center. With the collaboration of Nepal Flying Labs with DroNepal and Birat Nepal Medical Trust (BNMT), the project has been successfully supplying medical utilities from rural to center labs (Iamnepal, 2020).

1.2. Problem Statement

Due to harsh topography, the construction of roadways and railways in remote regions of Nepal is difficult and costly. So, UAVs can become a valid means of transport, especially for emergency medical supplies and disaster relief items in rural Nepal. It can also useful for rescue operations in mountains and agriculture. Recently, the use of UAVs is increasing in Nepal but they are mostly small drones and are limited to videography, surveillance and transport of low payload (<5 kg).

The design process of aircraft begins with weight estimation and initial sizing, which needs to be iterated to reach final design. Experimental verification of each change in configuration is costly and time-consuming. So, simulation of these changes would be more economical and effective until satisfactory configuration is obtained, which can then be validated experimentally.

1.2 Objectives

1.2.1 Main Objectives

To design a wing structure for a fixed-wing UAV targeted to carry 25 kg payload and perform FSI analysis of the wing structure for design validity and aerodynamic performance enhancement.

1.2.2 Specific Objectives

- To select the appropriate wing position and configuration.
- To select airfoil for the wing design.
- To find deformation and stress on wing structure using FSI.
- To compare lift to drag ratio of different wing configurations.

1.3 Assumptions and Limitations

- Maximum lift to drag ratio of the aircraft is assumed to be 15 during initial weight estimation.
- Design of control surfaces- flaps and ailerons should be done further to finalize the wing design.
- The flow is considered to be steady state as simulation is done for level flight at cruise condition.

- Only one-way FSI is carried out, which is suitable for preliminary analysis but may not accurately capture the dynamic interactions between wing structure and surrounding air.

CHAPTER TWO: LITERATURE REVIEW

2.1. History and Development of UAVs

The development in aviation accelerated after the historic first flight taken by Wright brothers in 1903, and unmanned aircrafts soon followed the suit undergoing major breakthrough in World war era. But the idea of automated mechanisms and flight was introduced more than 2000 years ago in ancient Greece and China.

Pythagoras, Archimedes and other scientists studied automated mechanisms for various applications. The first major contribution to the discovery of autonomous mechanisms is attributed to Archytas of Tarantas, southern Italy, from Pythagorean era. He implemented a set of geometrical concepts, thus creating the first UAV, as a mechanical bird (Figure 2.1), which could fly by a mechanism placed in the stomach, in 425 BC. (Valavanis, 2007)

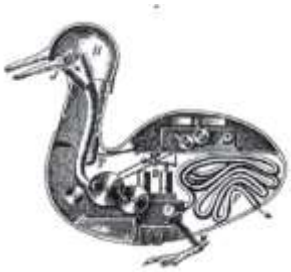

Figure 2.1: Mechanical bird (Valavanis, 2007)

In 400 BC, the idea of a device that can achieve vertical flight had been documented in China. In 1483, Leonardo Da Vinci designed an aircraft capable of vertical rise (Figure 2.2), considered by some experts as the ancestor of today's helicopter (Prisacariu, 2017). In 1508, he also designed a mechanical bird containing a double crank mechanism that descended along a cable (Rosheim, 2006).

Figure 2.2: Leonardo Da Vinci's Air Screw (Valavanis, 2007)

Later in 1754, Mikhail Lomonosov designed an axial impeller, and in 1783, Bienvenue Launoy designed a counter-model propeller (Dalamagkidis, Valavanis, & Piegl, 2012). George Cayley designed a carriage convertiplane, which remained only at the stage of idea as the propulsion systems gauge were only available for steam locomotives at that time. In 1840, Horatio Phillips designed a machine capable of vertical flight routes, which contained a miniature boiler to generate steam. Then, in 1860, Ponton d'Amécourt flew smaller helicopter models (Figure 2.3) powered by steam (Valavanis, 2007).

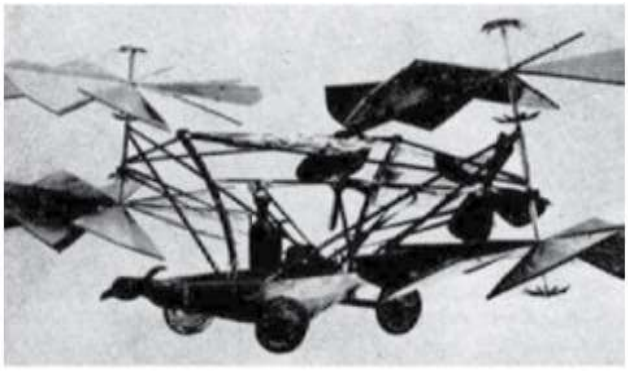

Figure 2.3: Ponton d'Amecourt's helicopters (Valavanis, 2007)

The major breakthroughs in the field of UAVs were made during World War era. The UAVs began to expand its field from military to humanitarian and commercial sectors, which can be summarized by the Figure 2.4.

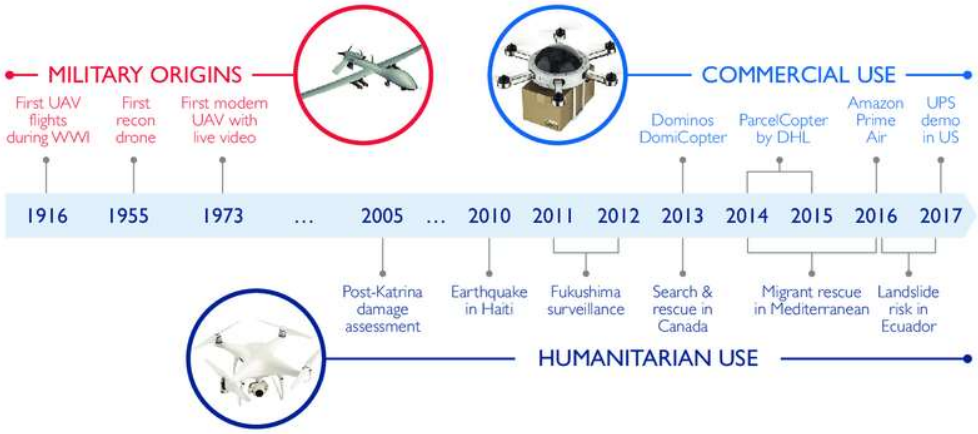

Figure 2.4: Evolution of UAVs from military origin to humanitarian and commercial use (Center for Accelerating Innovation and Impact, 2018)

2.2. Fixed wing UAV

2.2.1. Aerodynamic parameters

When air flows over an airfoil from leading edge to trailing edge, the pressure is distributed as shown in fig 2.8(b). The pressure difference between upper and lower surfaces of the aircraft causes the wings to rise.

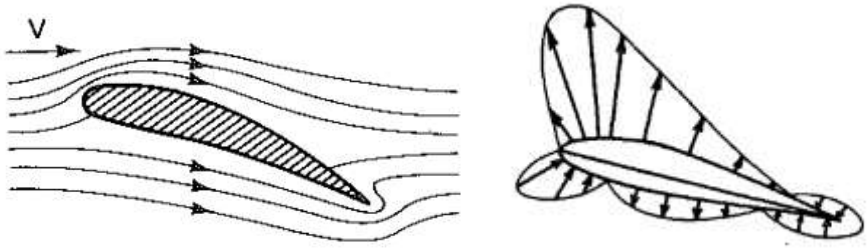

(a) (b)

Figure 2.5: (a) Flow over an airfoil & (b) Pressure distribution (Houghton & Carpenter, 2003)

The lift generated by a wing (L) can be calculated using formula:

$$L = \frac{1}{2}\rho V^2 S C_L \qquad \text{Equation 2.1}$$

Where, C_L = coefficient of lift of wing

S = wing area

V = relative velocity of air

Similarly, drag induced can be calculated as:

$$D = \frac{1}{2}\rho V^2 S C_D \qquad \text{Equation 2.2}$$

Where, C_D = coefficient of drag of wing

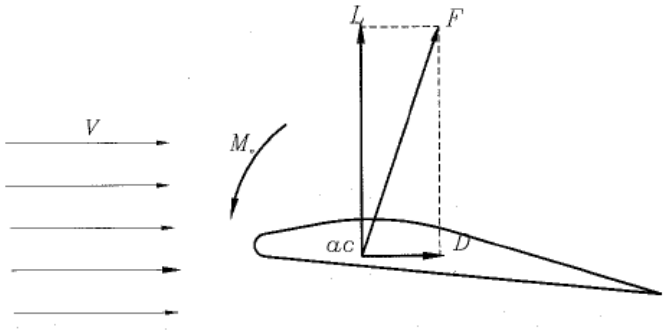

Figure 2.6: Lift, Drag and Pitching moment acting on a wing (Sadraey, 2013)

There are mainly four different forces acting on an aircraft:

- Thrust: force provided by propeller or propulsion system that pushes aircraft forward.
- Weight: downward force acting due to gravity.
- Lift: upwards force mostly generated by wings lifting the aircraft up.
- Drag: backwards force caused due to friction and aerodynamic pressure.

The three types of moment acting on an aircraft are as follows:

- Pitch: It is the rotation about side-to-side axis, i.e. nose up and down moments.
- Roll: It is the rotation about longitudinal axis.
- Yaw: It is rotation about vertical axis.

Some of the important aerodynamic parameters are:

- Angle of attack (α): It is the angle made by chord of an aircraft with relative wind direction.
- Aerodynamic center (ac): It is the point in the wing where pitching moments are independent of angle of attacks.
- Center of pressure (cp): It is the point in the wing where the resultant force acts.

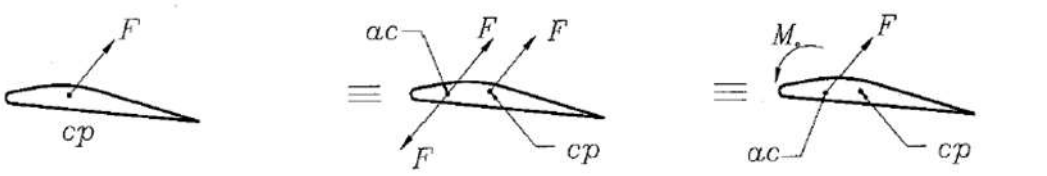

Force on pressure center Addition of two equal forces Force on aerodynamic center

Figure 2.7: Transfer of moment and force between ac and cp (Sadraey, 2013)

2.2.2. Characteristics graphs of airfoil

Variation of lift coefficient versus angle of attack

- Stall angle (α_s) is directly related to the flight safety. If it isn't controlled properly, the aircraft may spin or crash. So, higher stall angle is preferred while selecting the airfoil to ensure security.
- Maximum lift coefficient (C_{lmax}) usually occurs at the stall angle. The stall speed (V_s) is inversely proportional to the function of maximum lift

coefficient. So, higher C_{lmax} leads to the lower stall speed giving safer flight. Airfoil with maximum lift coefficient is desirable during airfoil selection.

- Zero lift angle of attack (α_0) is basically negative close to zero when no high lift device is employed. So, higher negative α_0 gives more lift at zero angle of attack. It is necessary for cruising flight for comfort flight.

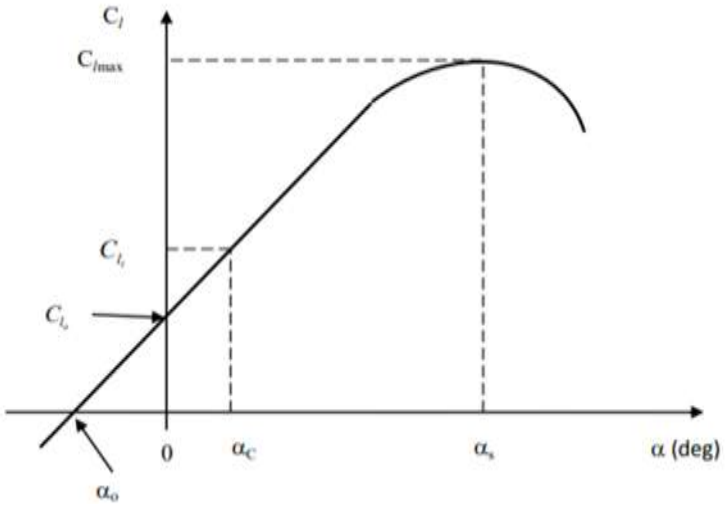

Figure 2.8: Variation of lift coefficient versus angle of attack (Sadraey, 2013)

- At ideal lift coefficient (C_{l_i}), minimum drag coefficient remains unchanged even for a significant change in angle of attack. Thus, cruise flight is done in this angle as close as possible.
- Higher lift coefficient at zero angle of attack (C_{l_0}) is preferred since it implies that we can produce positive lift even at zero angle of attack.
- Lift curve slope (C_{l_α}) gives the variation of lift coefficient with respect to the change in angle of attack.

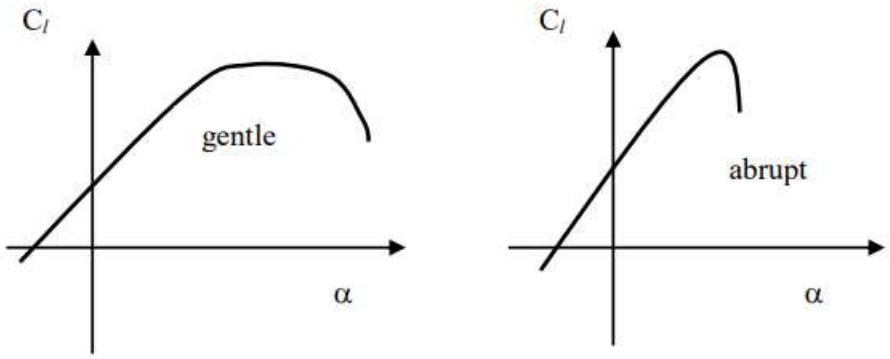

Figure 2.9: Lift curves after stall (Sadraey, 2013)

- Airfoil with gentle drop in lift after stall results safer stall from which pilot can recover. But it becomes uncontrollable if the lift curve is abrupt after stall angle of attack.

Variations of pitching moment coefficient versus angle of attack

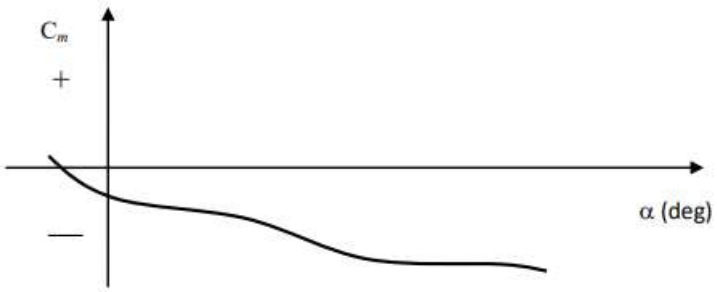

Figure 2.10: Variations of pitching moment coefficient versus angle of attack (Sadraey, 2013)

The slope of this graph is negative in the negative pitching moment (C_m) for typical range of angle of attack. Negative slope is desirable as it stabilize the flight, if it is disturbed by the gust. It is due to its moment in negative direction about y – axis i.e., aircraft nose will be pitched down.

Variation of drag coefficient as function of lift coefficient

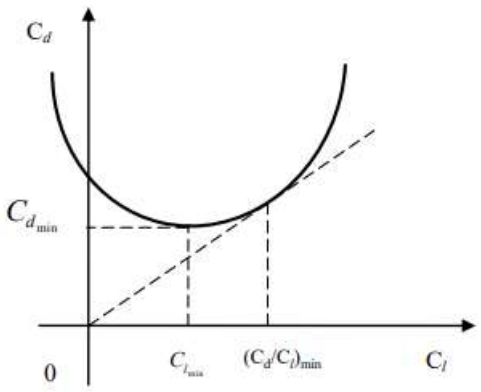

Figure 2.11: The typical variations of drag coefficient versus lift coefficient (Sadraey, 2013)

The lowest point of this graph is called minimum drag coefficient ($C_{d_{min}}$), which corresponds to the minimum drag. It correlates to the cost of flight so the airfoil with lower $C_{d_{min}}$ is more desirable.

A line drawn through the origin and tangent to the graph locates the point which gives minimum slope. It is of great importance as it indicates the flight situation that maximum C_l to C_d ratio is generated since $(C_d/C_l)_{min} = (C_l/C_d)_{max}$.

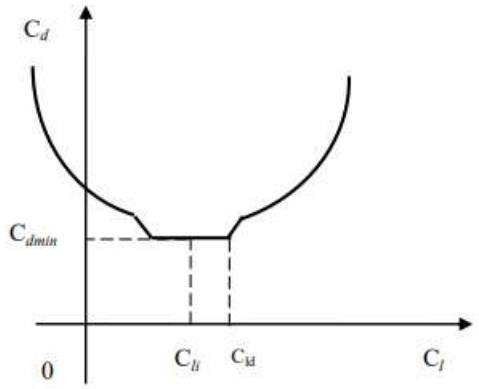

Figure 2.12: variations of Cl versus Cd for a laminar airfoil (Sadraey, 2013)

Fig 2.12 shows the typical variation of drag coefficient as function of lift coefficient for laminar airfoil. Its unique feature i.e., bucket shape of lower portion of graph, represents that (C_d)min will not vary over range of C_l. That means pilot can maintain low drag while changing the angle of attack i.e., it makes possible to keep low engine throttle low during cruising flight.

Middle point of bucket is ideal lift coefficient (C_l), while highest C_l in bucket region is referred as design lift coefficient (C_{l_d}). For other flight condition like loitering, pilot tries to fly at the point where lift coefficient is equivalent to C_{l_d}.

Variation of lift-to-drag ratio (C_l/C_d) as function of angle of attack

It is utilized during the process of airfoil selection. This graph has one maximum point where value of lift-to-drag ratio is highest at this point. The angle of attack corresponds to this point is the optimum candidate for loitering flight (α_l).

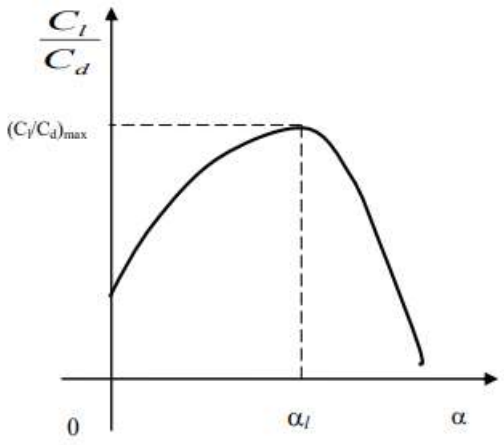

Figure 2.13: Typical variations of lift-to-drag ratio versus angle of attack (Sadraey, 2013)

2.3. Recent Research and Developments

In 1984, H. Sobieczky and A.R. Seebass provided a precise method of designing super-critical wing to compute the aerodynamic flow over the wing (Sobieczky & Seebas, 1984). In case of high-altitude and long-endurance, the airfoil design reached its level such that it can be tailored to specific mission where the highest-level performance can be achieved (Maughmer & Somerst, 1987). Andras Sobester et. al strongly supported the idea of getting baseline design was through initial estimation of maximum takeoff weight. In 2005, they also mentioned that the performance of aircraft depends on thrust to weight ratio and wing loading (Sobester, Keane, Scanlan, & Bressloff, 2005; Sobieczky & Seebas, 1984)

Around 2010, strength and stiffness analysis of UAV's wing was done using Finite Element Analysis (FEA) software ANSYS. Farrukh Mazhar & Abdul Munem Khan performed this analysis by applying the aerodynamic load as pressure function, which showed the use of reinforced composite material could be the effective material to sustain the aerodynamic loads. They also showed that Aluminum as material fulfilled the requirements and had considerable reduction in the weight (Mazhar & Khan, 2010). Airfoil design variable generated from Metric-based mathematical mode shape gave the high curvature region precisely. In 2014, Daniel J. Poole et. al concluded that those generated mode shape performed very well (Poole, Allen, & Rendall, 2015).

To avoid the tip-vortex, winglet came in the existence while improving the performance the wing of UAV. Computational Fluid Dynamics (CFD) was used to investigate the flow around the winglet of Medium Altitude Long Endurance (MALE) UAV. In 2014, P. Panagiotou and his team confirmed that there was considerable improvement in aerodynamic performance of UAV (Panagiotou, Kaparos, & Yakinthos, 2014). In 2015, for aerial photography, Dewi Anggraeni and his team designed and analyzed the medium range UAV for its flight performance. They found out that pusher configuration paid better stability and the airfoil NACA 4415 was selected based on analytical calculations and wind tunnel test results (Anggraeni, Hidayat, Pramutadi, & Soemaryanto, 2015).

In 2016, Maxim Tyan and his team discovered fixed wing aircraft provides greater efficiency for cruising flight. The only problem was high power consumption causing short operational time in case of hybrid electric UAV (Tyan, Nguyen, Lee, & Kim, 2016). While considering the aerodynamic design of MALE UAV, in 2016, P. Panagiotou et. al developed four UAV concepts and studied their UAV's physical parameters then combined their optimal feature in one design. That design yielded the significant endurance compared to initial those designs (Panagiotou, Kaparos, Salpingidou, & Yakinthos, 2016). In 2017, Jesús Manuel et. al studied the optimum location of propulsive system considering Center of Gravity (CG), Center of Pressure (CP) and Aerodynamic Center (AC) of UAV. They found out that the location at front reduces negative turbulence and made easy to locate CG, CP and AC. They also concluded that decreasing propeller's size and increasing blade's number reduce the noise without compromising performance (Muñoz & Tilvaldyev, 2017). Kristofer Gryte and his team made model for the Fixed-wing UAV considering aerodynamic nature using numerical model, which was later validated by wind tunnel testing results in 2018 (Gryte, et al., 2018). In 2020, R Pavithran R et. al made prototype of Fixed-wing UAV for medical purpose which used autonomous module for flight and parachute for payload delivery (Pavithran, et al., 2020).

Similarly, Tosmaz Goetzendorf-Grabowski and his team analyzed different copter configurations for light-weight UAV for emergency medical service. They found out that the co-axial quadcopter configuration crossed with convectional airplane was better, giving best performance of all other configurations (Goetzendorf-Grabowski, Tarnowski, Figat, Mieloszyk, & Hernik, 2020). Guillaume J.J. and his team reviewed

the design for Hybrid and Convertible Vertical Take-Off and Landing (VTOL) in 2021. The simplest design they found out was tail-sitter type with either two propeller and two elevons, or four propellers and no elevons for hybrid VTOL UAV (Ducard & Allenspach, 2021). Comparing different type of electric propulsion systems of Hybrid wing VTOL UAV in 2021, Jianan Zong and et. al found out the turboelectric and hybrid system exhibited the better performance and lower manufacturing cost. Among hybrid system, they concluded that series hybrid was better (Zong, Zhu, Hou, Yang, & Zhai, 2021). In the same year, Chiranjivi Dahal and his team designed and analyzed the propeller for high-altitude search and rescue UAV. They commented that commercially available UAV were not good enough at high altitude. So, they decided to design thrust optimized blade for high altitude and performed thrust analysis (Dahal, Dura, & Poudel, 2021).

2.4. Benchmarking of UAVs

Different UAVs available in market and their properties were studied. The UAVs that have similar requirements to ours were narrowed down, so we can compare our calculated values with them and get surface idea of whether our design is plausible or not.

Table 2.1: Benchmarking of UAVs

No.	UAV	Weight (kg)	Payload (kg)	Endurance (hr)	Range (km)	Ceiling (m)	Speed (km/hr)	Wing Span (m)	Engine	Power (kW)
1	AAI RQ-7 Shadow	90	25.3	6	200	4572	194.5	4.27	rotary	28
3	Lockheed MQM-105 Aquila	100	52	3	100	4500	210	3.89	two-stroke	18
4	PRIMOCO	100	30	15	2000	3300	130	4.85	2-cylinder	
5	Crecerelle	120	35	6	59	3353	246	3	piston	20
6	Pioneer	125	64	5	373	4,572	175	5	two-stroke	22
7	Cypher	136	20	3	30	1,524	148	0	rotary piston	39
8	Alliant RQ-6 Outrider	136	27	6		4600	200	3.383		37

2.5. Research Gap

Most of the drones commercially available now have a payload capacity of 1-5 kg and have limited range. Further, they are highly affected by the weather and wind conditions and have low flight altitude and range, which is not too favorable for the mountainous and remote regions like Nepal. This has limited us from realizing the full potential of UAVs in the activities ranging from transport of bulky equipment, medical kits, disaster relief items, emergency oxygen cylinders in high altitude regions, carrying out rescue missions and so on. In this project, we design wing structure for a medium range fixed wing UAV and optimize it to obtain high lift to drag ratio using Fluid-Structure Interaction (FSI) simulation, which can be used as a basis for actual prototyping of UAV.

CHAPTER THREE: METHODOLOGY

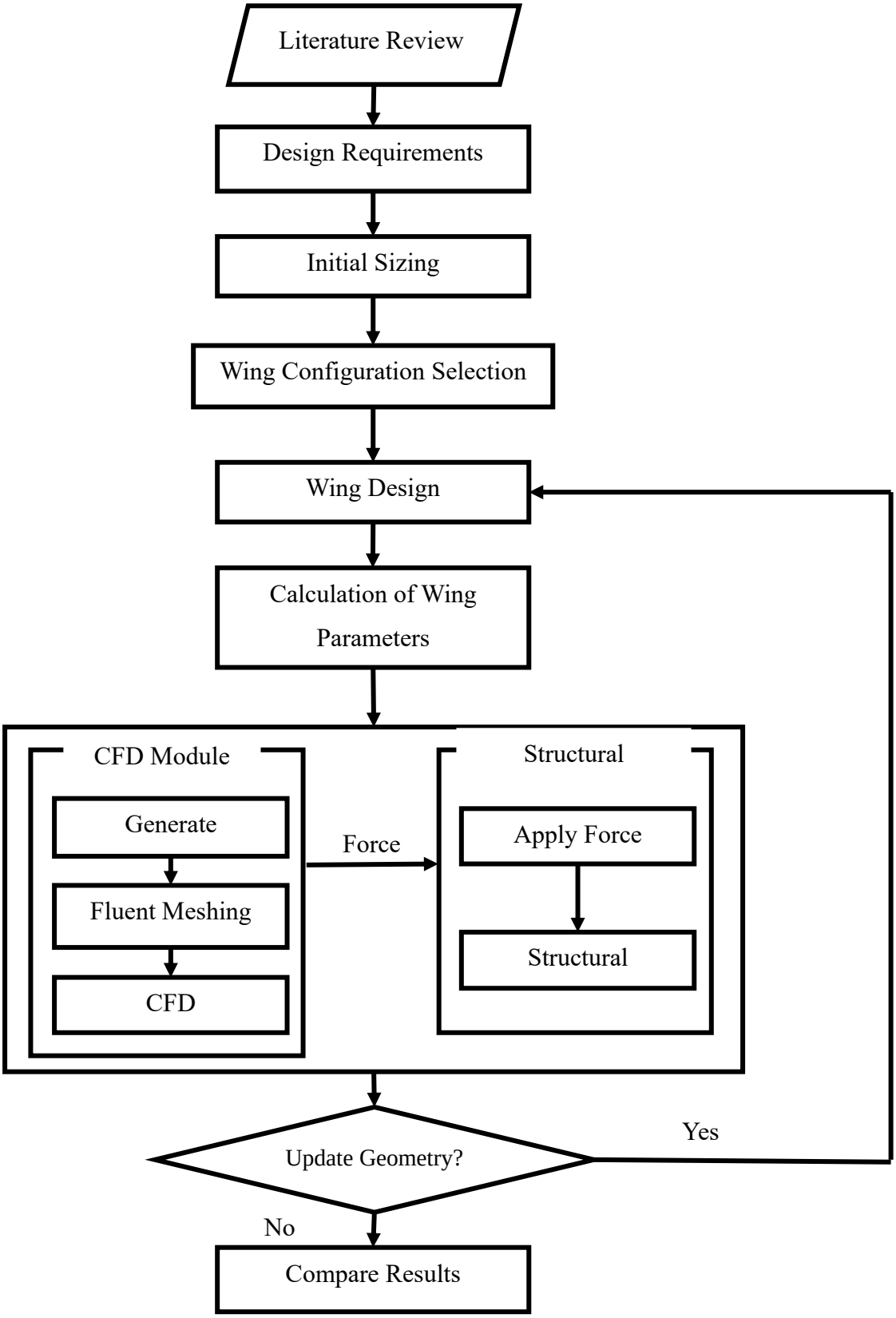

Figure 3.1: Methodology Flowchart

3.1. Literature Review

A prior literature review was done to know the history and recent developments of UAV. The design and calculations of parameters and components related to fixed wing UAV was studied. Different software required for modelling wing structure (CATIA, SOLIDWORKS) and Aerodynamic and structural analysis (XFLR5, ANSYS) of wing structure was reviewed. The related research for analytical calculations and software use was reviewed to gather knowledge on how to proceed with the project. We decided to generate 3D model of wing structure using SOLIDWORKS, initial analysis of aerodynamics using XFLR5 and fluid-structure interaction on ANSYS Fluent.

3.2. Flight Conditions and Design Requirements

Input design parameters are range, lift to drag ratio, endurance, cruising altitude, payload weight, cruise speed and the aspect ratio. These will serve as a basis for the analytical calculations and iterative initial sizing. (TURANOĞUZ, 2015) We selected custom requirements for the UAV as mentioned below:

- Payload weight: 25 kg
- Altitude: 3000 meters above sea level
- Range: 150 km
- Cruise Velocity: 40 m/s
- Endurance: 2 hr.

3.3. Analytical Calculations and Initial Sizing

The analytical calculations were done as per existing literatures, mainly “Aircraft Design: A Conceptual Approach”. The design process was handled by generating an excel file in which the design parameters cruise speed, aspect ratio, endurance, range, etc. was included. The iterative calculations were done to depict airfoil type, wing loading, engine selection, wing geometries, performance parameters and performance coefficients.

3.4. Selection of Wing Configuration

The most suitable wing configuration (wing placement, sweep angle, dihedral and planform shape) was selected after briefly studying their properties and weighing pros

and cons. This step may be revisited if any adjustment is to be made after the simulation is done.

3.5. Airfoil Selection

Reynolds number of aircraft during different flight conditions: takeoff, cruise and stall was calculated and different airfoils suited for our application was chosen from website: http://airfoiltools.com/ and their aerodynamic properties were compared to select best airfoil for the wing design.

3.6. Design of Wing Structure

A CAD model of Wing structure including skin, ribs and spar was generated using SOLIDWORKS software. Performance and stability analysis was done using XFLR5 to validate the initial wing design and make required adjustments. Lift and drag coefficients, pitching moment, efficiency were obtained from XFLR5, which were used to check sufficiency of design. We also checked if the parameters are within flight envelope to ensure the conditions are under safe range of operation.

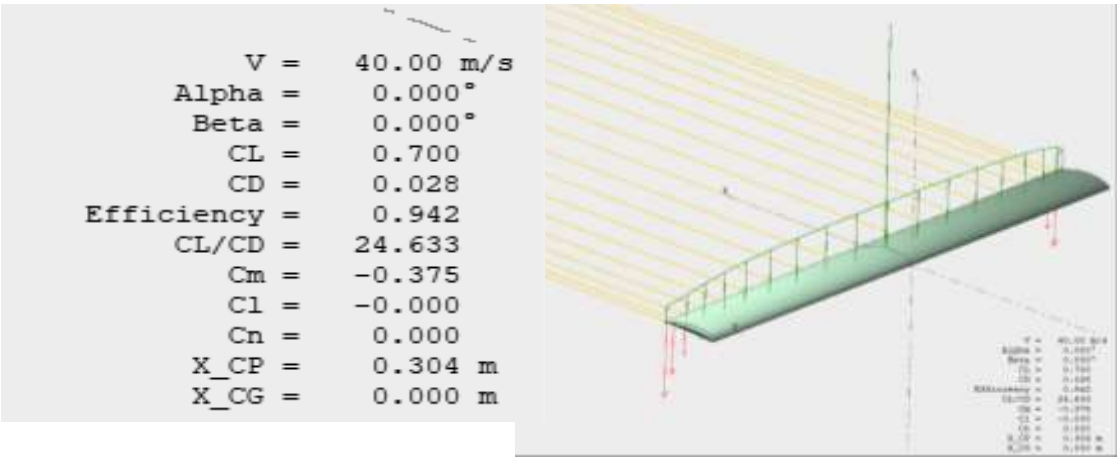

Figure 3.2: Performance analysis of wings using XFLR5

3.7. Fluid Structure Interaction Analysis

An aircraft is in a state of combined load from pressure and temperature. To predict the response of fluid and effect of mechanical loading on structure of aircraft, FSI

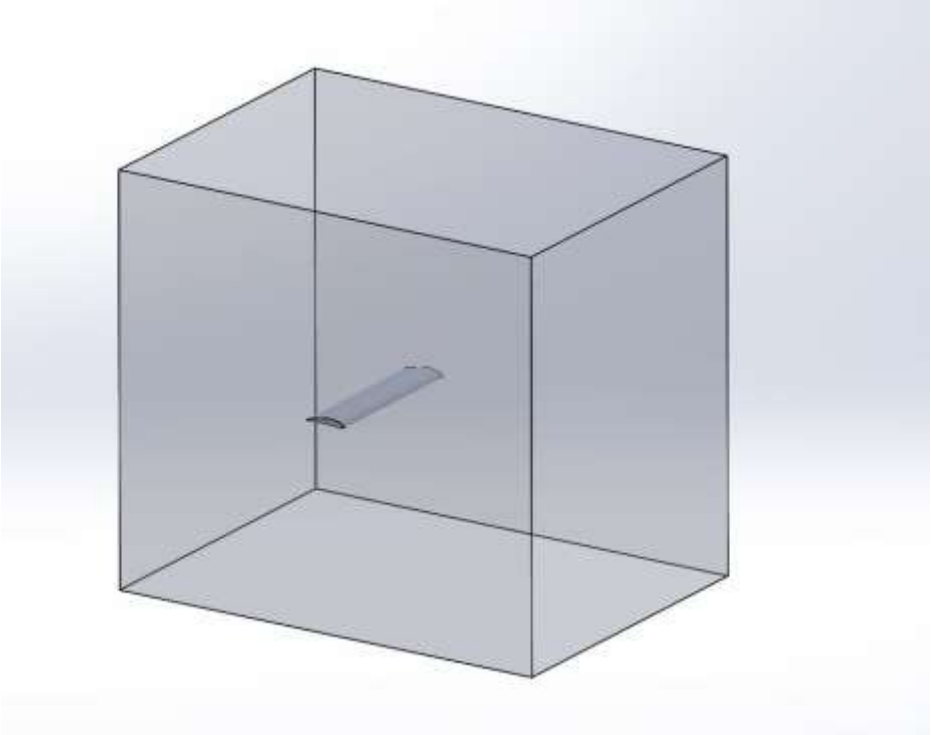

Figure 3.3: Fluid domain over wing surface (Dimension: 5.7×5.7×3.5) m

simulation was carried out on ANSYS. The geometry STEP file from SOLIDWORKS was imported and shared between fluid and structural modules. The fluid domain was created using ANSYS Design Modeler. The size of the fluid domain is 10 times the chord length on each sides and has 1 m additional depth than the wing span.

Aluminium 2024-T3 and air were setup as materials in Engineering data tab. The properties of Aluminium 2024-T3 at room temperature (25 °C) are:

Density = 2768 kg/m^3

Young's Modulus = 73040 MPa

Thermal Conductivity = 126.1 W/m.°C

Tensile Yield Strength = 328.5 MPa

Ultimate Tensile Strength = 427.9 MPa

3.7.1 Meshing

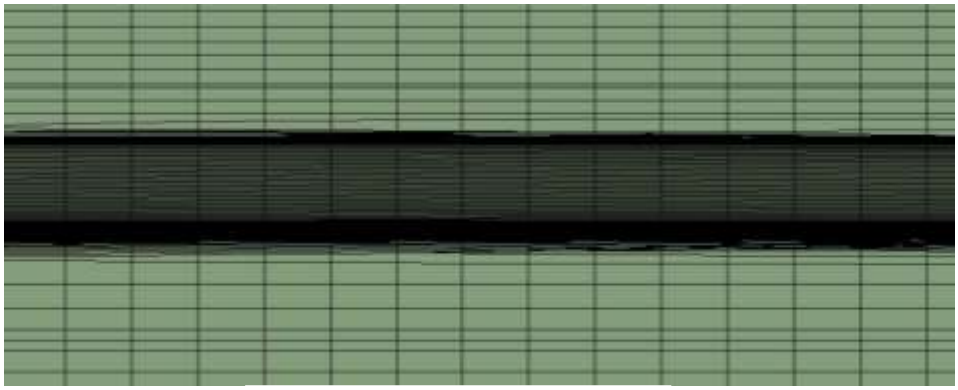

(a) Sectional side view

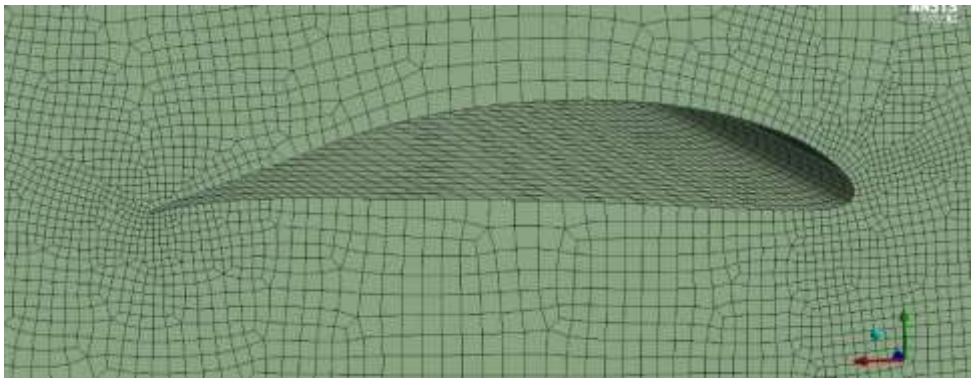

(b) Front View (at wing root)

Figure 3.4: Meshing of Fluid domain

For the discretization of fluid domain, Fluent meshing was used. Here, sizing, mapping and multizone methods were used to generate uniform good quality mesh.

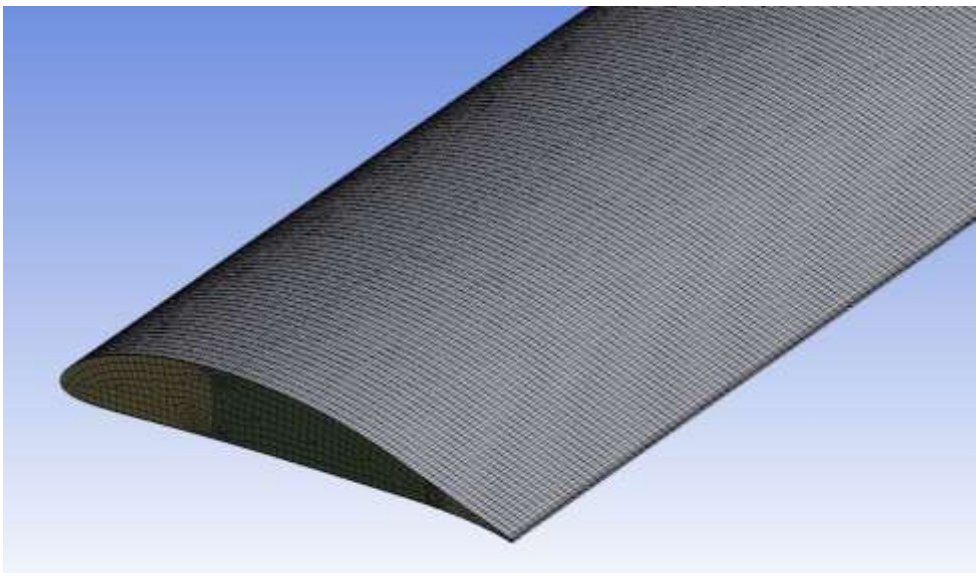

Figure 3.5: Structural mesh of wing-structure

Similarly, structural mesh was generated using ANSYS Mechanical. The mesh was refined using sizing and mapping features.

Table 3.1: Mesh Parameters

Parameters	Fluent	Static Structural
Mesh Type	Hex	Hex
No. of nodes	429414	499386
No. of elements	155773	139434

After refining mesh and setting up required inlet and boundary conditions, CFD analysis was carried out using Fluent module in ANSYS and the pressure effect obtained from the analysis was imported to ANSYS Static Structural to carry out structural simulation.

3.7.2. Setup Parameters

For Fluent solver,

Inlet Boundary Condition: velocity = 40 m/s

Outlet Boundary Condition: gauge pressure = 0 Pa

Solution methods:

- Pressure-Velocity Coupling: Scheme = Coupled
- Spatial Discretization: Gradient = Least square cell based
  Pressure = second order
  Momentum = Second order upwind
  Turbulent Kinetic energy = First order upwind
  Specific Dissipation Rate = First order upwind

For Mechanical ADPL solver (Static Structural Analysis),

- Fixed Support: Spar surfaces at the wing root
- Force: Gravity (1196.82 N) vertically downwards
- Imported load: Pressure load over the entire wing-air interface

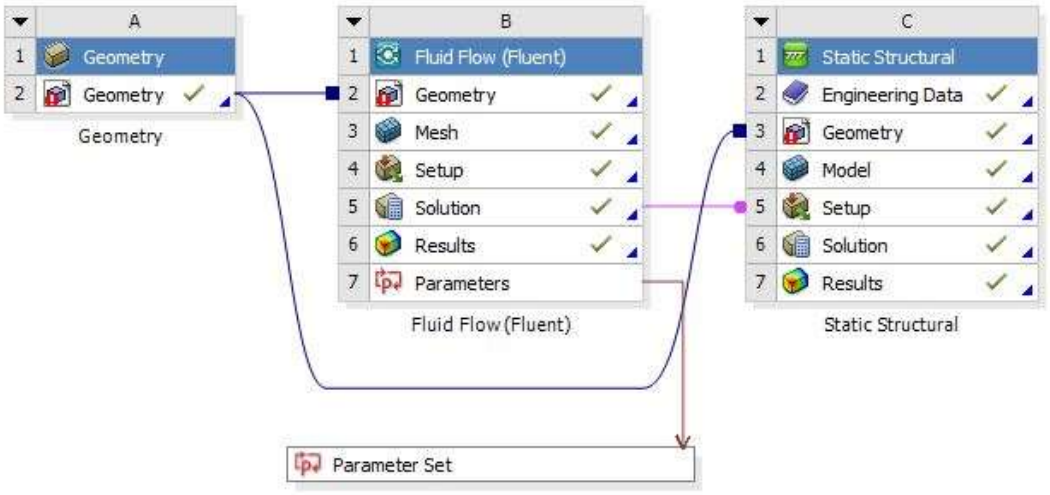

Figure 3.6: Project Schematic for one-way FSI analysis on ANSYS

3.8. Comparison of Results

We performed a total of 15 FSI simulations by changing chord length, wingspan and dihedral angle of the wing. We wanted to select the best design point for the wing structure having highest lift to drag ratio (C_L/ C_D). Analysis of Mean (ANOM) was used to determine how significant the difference between values of L/D were from the mean for each design point and which parameter has a significant impact on L/D.

CHAPTER FOUR: RESULTS AND DISCUSSION

4.1. Initial Sizing

The initial estimation of weight of an aircraft is done in the beginning by the initial estimation of range and payload.

4.5.1. Gross Weight Estimation

It is the first process in design of a fixed wing UAV. The design take-off gross weight is given by the formula:

$$W_o = W_{empty} + W_{payload} + W_{fuel} + W_{crew} \qquad \text{Equation 4.1}$$

The only unknowns are fuel weight and empty weight of the aircraft. To simplify the calculation, the equation (1) can be represented as:

$$W_o = W_{crew} + W_{payload} + \left(\frac{W_f}{W_o}\right) W_o + \left(\frac{W_e}{W_o}\right) W_o$$

$$W_o - \left(\frac{W_f}{W_o}\right) W_o - \left(\frac{W_e}{W_o}\right) W_o = W_{crew} + W_{payload}$$

$$W_o = \frac{W_{crew} + W_{payload}}{1 - \left(\frac{W_f}{W_o}\right) - \left(\frac{W_e}{W_o}\right)} \qquad \text{Equation 4.2}$$

Where,

$\left(\frac{W_e}{W_o}\right) =$ empty weight fraction, $\left(\frac{W_f}{W_o}\right) =$ fuel weight fraction

$W_{crew} = 0$ (For UAV)

$W_{payload} = 25\text{kg}$ (Design Requirement)

The empty weight fraction for different types of aircraft can be calculated using table 4.1. It gives the coefficients to calculate the necessary empty weight ratio for different kinds of aircraft.

Table 4.1: Empty Weight Fraction for different aircrafts (Raymer D. P., 2018)

$W_e/W_o = AW_o^C K_{vs}$	A	C
Sailplane – unpowered	0.86	-0.05
Sailplane – powered	0.91	-0.05
Homebuilt – metal/wood	1.19	-0.09
Homebuilt – composite	0.99	-0.09
General aviation – single engine	2.36	-0.18
General aviation – twin engine	1.51	-0.10
Agricultural aircraft	0.74	-0.03
Twin turboprop	0.96	-0.05
Flying boat	1.09	-0.05
Jet trainer	1.59	-0.01
Jet fighter	2.34	-0.13
Military cargo/bomber	0.93	-0.07
Jet transport	1.02	-0.06

K_{vs} = variable sweep constant = 1.04 if variable sweep

= 1.00 if constant sweep

Assume, W_o = 100 Kgs

Since our intended aircraft is similar in operation to military cargo aircraft,

$$\frac{W_e}{W_o} = AW_o^C K_{vs} = 0.93 \times 100^{-0.07} \times 1 = 0.6737$$

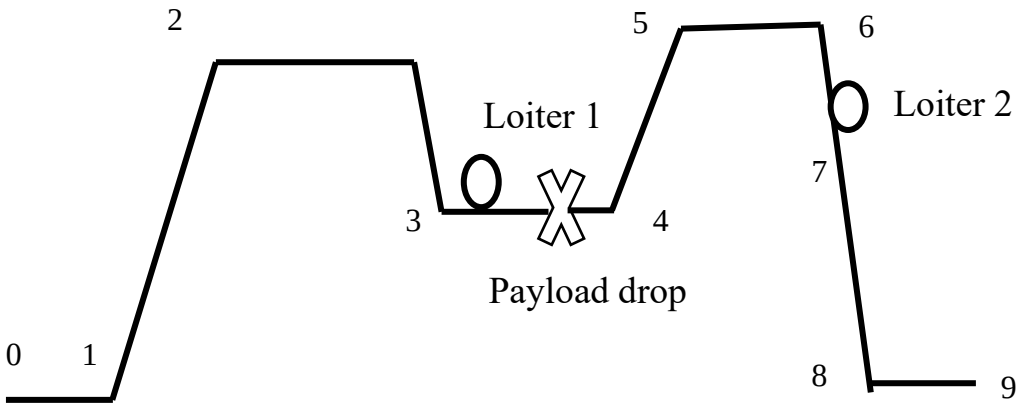

Figure 4.1: Mission profile for intended UAV (Air Superiority)

For calculating fuel weight fraction, we need to estimate a mission profile. We want our UAV to drop payload to remote location while still at air and land safely to the nearest available runway. Air superiority mission profile is best suited for this purpose. For fuel weight fraction estimation, we supposed the payload is not dropped to ensure that the UAV can return safely if payload couldn't be dropped for some reason. So, the weight dropped is equivalent to fuel used.

We need to calculate weight ratios at each mission states of the profile. 'W_n' represents the weight of the aircraft at different mission points 'n' as shown in Fig. 4.1. In our simple sizing method, we ignore descent for payload drop, assuming that the cruise ends with a descent and distance travelled during the descent is part of the cruise range.

Table 4.2: Weight Ratios for Different Mission States

Weight Ratios	Mission state
W_1 / W_o	Warmup and takeoff
W_2/W_1	Climb
W_3/W_2	Cruise 1
W_4/W_3	Loiter 1
W_5/W_4	Climb 2
W_6/W_5	Cruise
W_7/W_6	Loiter 2
W_8/W_7	Descent
W_9/W_8	Land

For warmup, climb, descent and landing, the fractions were taken from historical mission data. These are the averaged value of data taken from previous airlines operation data, military missions and other flight operations, which can give general idea on fuel consumption pattern of aircrafts.

Table 4.3: Historical Mission Data for Weight Ratios (Raymer D. P., 2018)

	(W_i / W_{i-1})
Warmup and takeoff	0.970
Climb	0.985
Landing	0.995

For cruise, the weight ratios were calculated using the following equation (Raymer D. P., 2018):

$$\frac{W_i}{W_{i-1}} = \exp\frac{-RC}{V(L/D)} \qquad \text{Equation 4.3}$$

Where,

$R = \text{range}$, $C = \text{specific fuel consumption}$

$V = \text{Velocity}$, $\frac{L}{D} = \text{Lift to Drag Ratio}$

The value of C is calculated from Table below considering variable pitch Piston Prop:

Table 4.4: Propeller Specific Fuel Consumption (Raymer D. P., 2018)

Propeller: $\mathbf{C = C_{bhp}V/550\eta_p}$ **Typical C_{bhp} and η_p**	**Cruise**	**Loiter**
Piston-prop (fixed pitch)	0.4/0.8	0.5/0.7
Piston-prop (variable pitch)	0.4/0.8	0.5/0.8
Turboprop	0.5/0.8	0.6/0.8

From table 4.4, for variable pitch piston-prop aircraft, $C_{bhp}/\eta_p = 0.4/0.8$

Where, $\eta_p = \text{propeller efficiency}$

C_{bhp} = cylinder brake horsepower of engine (hp)

V= velocity in feet per seconds = 131.23 ft/s

$$C = \frac{C_{bhp}V}{550\eta_p} = \frac{0.4\times131.23}{550\times0.8} \times \frac{1}{3600} = 3.314 \times 10^{-5}\ s^{-1}$$

$$\text{Range (R)} = 150\text{km} = 150 \times 91000 \times 3.28084\ \text{ft} = 492126\ \text{ft}$$

$(L/D)_{max} = 15$ (assumption)

For propeller aircrafts during cruise, L/D = $(L/D)_{max}$ (Raymer D. , 2018)

$$\frac{W_i}{W_{i-1}} = \exp\frac{-RC}{V(L/D)} = \exp\frac{-(492126\times3.314\times10^{-5})}{131.23\times(15)} = 0.992$$

Similarly, for loiter, the weight ratios were calculated using the following formula (Raymer D. P., 2018):

$$\frac{W_i}{W_{i-1}} = \exp\frac{-EC}{(L/D)} \qquad \text{Equation 4.4}$$

Where, $E = \text{Endurance or Loiter Time}$

Endurance $(E) = 2$ hr = 7200 s

$$C = \frac{0.5\times131.23}{550\times0.8}\times\frac{1}{3600} = 4.14\times10^{-5}\ s^{-1}$$

For propeller aircraft during loiter, L/D = 0.866 $(L/D)_{max}$ (Raymer D. P., 2018)

Then, the weight fraction for loiter is given by:

$$\frac{W_i}{W_{i-1}} = \exp\frac{-EC}{(L/D)} = \exp\frac{-(7200\times4.14\times10^{-5})}{0.866\times15} = 0.977$$

The fuel fraction for descent during landing is taken from historical mission data, which ranges from 0.990-0.995 (Raymer D. P., 2018). So, we take 0.993 for initial estimation.

The weight fraction in different mission stages are mentioned in table 4.5.

Table 4.5: Calculated Weight Ratios

Weight Ratios	Symbol	Value
Warmup and Takeoff	W_1/W_o	0.97
Climb 1	W_2/W_1	0.985
Cruise 1	W_3/W_2	0.992
Loiter 1	W_4/W_3	0.977
Climb 2	W_5/W_4	0.985
Cruise 2	W_6/W_5	0.992
Loiter 2	W_7/W_6	0.977
Descent	W_8/W_7	0.993
Land	W_9/W_8	0.995

Then, Ratio of final weight to Initial weight is given by:

$W_9/W_0 = 0.97 \times 0.985 \times 0.992 \times 0.977 \times 0.985 \times 0.992 \times 0.977 \times 0.993 \times 0.995 =$

Then, $W_9/W_0 = 0.876$

Thus, Mission Fuel Fraction $= 1 - W_9/W_0$

$= 0.124$

According to (Raymer D. , 2018), 6% extra fuel needs to be added for reserved and trapped fuel.

Then, Fuel weight fraction $\left(\frac{W_f}{W_o}\right) = 1.06 \times 0.126 = 0.1314$

Finally, Takeoff Weight $W_o = \frac{25}{1-0.1314-0.6737}$

Thus, $W_o = 128.27$ Kgs

With an initial approximation of 100 Kgs, the calculated takeoff weight is 127.61 Kgs. Iterative calculation was performed in excel to find W_o as shown in table 4.6.

Table 4.6: Iterative Gross Takeoff Weight Estimation

Estimated W_o	(W_e / W_o)	Calculated W_o
100 Kgs	0.6737	128.27 Kgs
125 Kgs	0.6633	121.62 Kgs
122 Kgs	0.6644	122.45 Kgs

From the table, we approximate the initial weight of the UAV to be 122 Kgs.

4.2. Wing Configuration

It is imperative in the conceptual design phase to evaluate the competing design concepts and establish our performance goals, which will be practical and achievable. Here we have compared different wing configurations and selected the most suitable one to move forward.

Table 4.7: Selection of Wing Configuration

Configuration	Selection	Reason
Placement	High	Simplicity of design, high ground clearance
Dihedral	As per further analysis (0 to 2 degrees for high wing placement)	To maintain balance between Maneuverability and Lateral stability
Sweep angle	Not needed	Intended aircraft is low subsonic (Mach number < 0.6)
Planform shape	Constant chord	Simple, economic

Table 4.8: Dihedral Guidelines ((Raymer D. P., 2018)

	Wing Position		
	Low	Mid	High
Unswept (civil)	5 to 7	2 to 4	0 to 2
Subsonic swept wing	3 to 7	-2 to 2	-5 to -2
Supersonic swept wing	0 to 5	-5 to 0	-5 to 0

Since the aircraft is unswept with high wing placement, dihedral = 0 to 2 degrees.

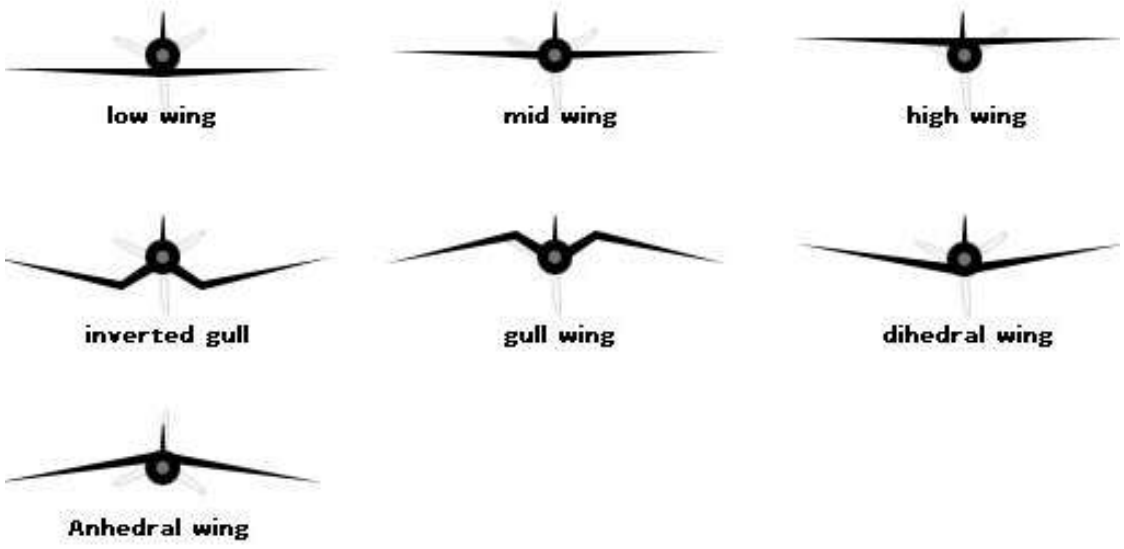

Figure 4.2: Different Wing configurations (Sweta, n.d.)

4.3. Wing Parameters Calculations

4.3.1. Wingspan and Wing Area

The first estimate of wingspan and wing area can be calculated using empirical scaling laws. This will be validated with benchmarking data and numerical simulations and updated along the project.

Over a large range of weight, birds and aircraft basically follow the power laws for wingspan and wing area, which is shown in Fig. 4.3.

For wingspan, we have for aircraft (14% mean relative error of regression), (Liu, 2006)

$$b = 0.462W^{\frac{1}{3}} \qquad \text{Equation 4.5}$$

Similarly, for wing area, the scaling laws for aircraft (30% mean relative error of regression), (Liu, 2006)

$$S_{wing} = 0.0262W^{\frac{2}{3}} \qquad \text{Equation 4.6}$$

Where, b= Wingspan of aircraft,

W = Mean aircraft weight, and

S_{wing} = Wing Area of aircraft.

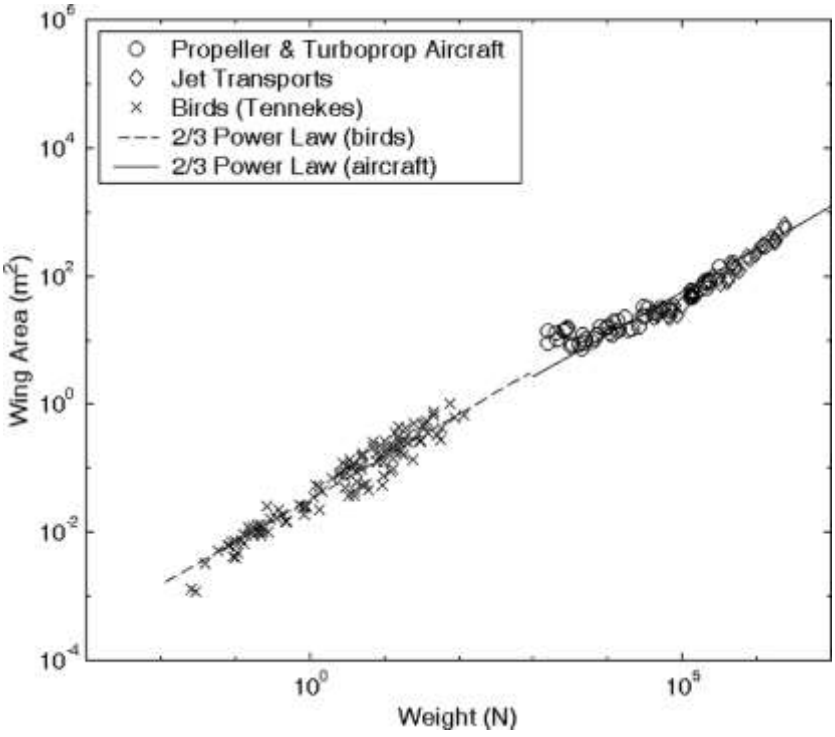

Figure 4.3: Wing Area as a function of Weight (Liu, 2006)

In our case,

Maximum Takeoff Weight (W_o) = 122 kgs

Empty Weight (W_{empty}) = 81 kgs

Mean aircraft weight, $W = \frac{W_o + W_{empty}}{2} = \frac{122+81}{2}$ = 101.5 kg = 995.715 N

We use mean aircraft weight as it represents typical operating weight of aircraft, which provides more optimized design. Maximum takeoff weight will will result in overly conservative design in this case.

Then, Wingspan, $b = 0.462W^{\frac{1}{3}} = 0.462 \times (995.715)^{\frac{1}{3}}$

That gives, $b = 4.61$ m

Also, Wing Area, $S_{wing} = 0.0262W^{\frac{2}{3}} = 0.0262 \times (1325.35)^{\frac{2}{3}}$

That gives, $S_{wing} = 2.61\ m^2$.

4.3.2. Stall Speed (V_{stall})

Stall speed is slowest speed a plane can fly to maintain level flight. Normally, when a plane slows down it makes less lift.

$$W = L = q_{stall} S C_{Lmax}$$

$$\frac{W}{S} = \frac{1}{2}\rho V_{stall}^2 C_{Lmax} \qquad \text{Equation 4.7}$$

Where,

$\frac{W}{S} = \text{Wing Loading}$, $\rho = \text{air density}$

$V_{stall} = \text{Stall Velocity}$, $C_{L_{max}} = \text{Max. Coefficient of Lift}$

Maximum lift coefficient is assumed to be 2.2 ($C_{L_{max}} = 2.2$), so that aircraft can be suitable for short takeoff and landing (STOL), which can be useful in remote hilly regions with short runway length. Typically, lift coefficient of lift higher than 2 is required for STOL operations.

We have, $\frac{W}{S} = \frac{122}{2.61} = 46.74\ kg/m^2 = 458.55\ N/m^2$,

$\rho = 1.19\ kg/m^3$ (At sea level at 25°C)

Then, stall velocity of aircraft at sea level is:

$$V_{stall} = \sqrt{\frac{458.55 \times 2.2}{1.19 \times 1.8}} = 21.7\ m/s$$

4.4. Airfoil Selection

First, we should calculate the Reynold's number during flight to narrow down the search of airfoil. There are different velocities at different stages of flight, but typical range of speed can be analyzed considering stall speed and cruise speed.

4.4.1 Range of Re

The Reynold's number (Re) can be calculated from the formula:

$$Re = \frac{Vl}{\upsilon} \qquad \text{Equation 4.8}$$

Where, V = velocity of aircraft

υ = kinematic viscosity of fluid

l = chord width/ characteristic length

Re during Cruise:

At cruise, elevation is assumed 10,000ft and cruise velocity is 40m/s. Then,

$$Re = \frac{Vl}{\upsilon} = \frac{40 \times 0.566}{1.863 \times 10^{-5}} = 1{,}215{,}244$$

Re during Stall:

During takeoff, the aircraft is typically at high angle of attack, which can increase the risk of stalling. So, considering stall behavior at sea level, i.e. during takeoff, Re can be calculated as:

$$Re = \frac{Vl}{\upsilon} = \frac{21.7 \times 0.566}{1.461 \times 10^{-5}} = 840{,}670$$

Wortmann airfoils work best for low Reynolds number and low Mach number aircrafts i.e. for Re, from 500,000 to 3,000,000 (McMasters & Henderson).

4.4.2 Comparison of different WORTMANN airfoils and selection of the best one

The comparison between different Wortmann airfoils was done with the help of Airfoil Tools.

Table 4.9: Comparison of different airfoils (Airfoil Tools, 2022)

Airfoils	FX 76-MP-140	FX 63-137	FX 72-MS-150A
Max cl/cd At Re= 1,000,000	181.6 at α= 3.75degree	132.5 at α= 2.25degree	160.2 at α= 7.5 degree
Max cl At Re= 1,000,000	1.75 at α= 13 degree	1.8 at α= 12.5 degree	1.8 at α= 8 degree
Min cd At Re= 1,000,000	0.008 at α= 0 degree	0.009 at α= 0 degree	0.01 at α= 1 degree
Graph smoothness	Smooth	Smooth	Rough

Among these compared airfoils, the best airfoil to give maximum C_l/C_d ratio was **Wortmann fx-76-mp-140** airfoil with maximum thickness of 14% at 33.9% of chord (Airfoil Tools, 2022).

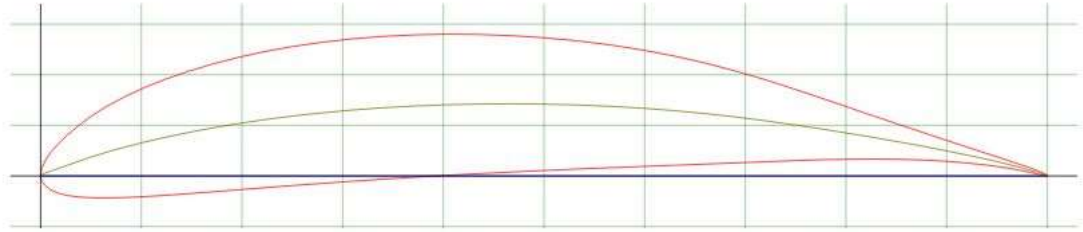

Figure 4.4: Airfoil profile of different Wortmann fx-76-mp-140 airfoil (generated by Airfoil Tools)

From fig 4.5, we find that maximum C_l/C_d of the airfoil is at around 5 degrees angle of attack. The coefficient of drag is low at angle of attack range of -5 to 5 degrees. It shows that 5 degrees angle of attack is favorable for cruise condition.

Maximum lift coefficient is 1.75 observed at 13 degrees angle of attack, which is the stall angle of attack of the airfoil. This is lower than assumed maximum lift coefficient of 2.2, but it can be achieved using high lift devices such as flaps. The zero coefficient of lift is at around -8 degrees angle of attack, which means the airfoil can't generate lift below this angle of attack. The shape of lift curve after stall is gentle, which means that the stall results are safer and gives controller enough time to recover.

The positive slope of C_m vs angle of attack curve may seem like a disadvantage as the airfoil has nose-down at higher angles of attack, which can make it difficult to maintain control. However, this can be beneficial in certain situations such as recovering from a stall or low speed and high lift operations. Since our aircraft is low speed, this is an advantage.

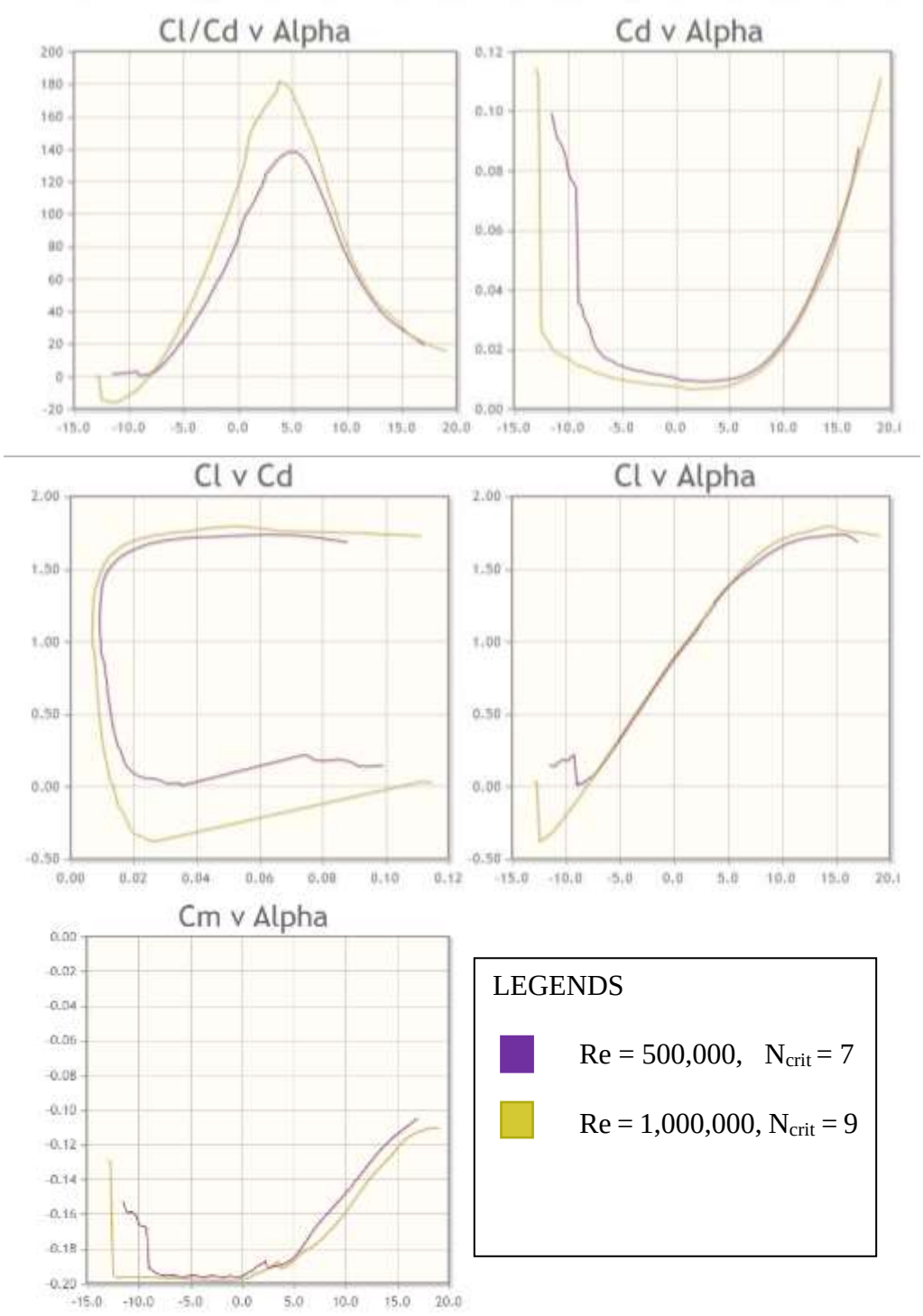

Figure 4.5: Characteristics graphs of Wortmann fx-76-mp-140 airfoil (generated by Airfoil Tools)

4.5. Initial 3D Model of Wing Structure

Wing parameters have already been calculated, so now we need to calculate the dimensions and parameters of supporting structures- ribs and spar.

4.5.1. Ribs

The number of ribs can be calculated using formula (Gudmundsson, 2014)

$$N_{rib} \approx \text{INT}\left(\frac{b}{C_{avg}}\right) + 1 \qquad \text{Equation 4.9}$$

Where, INT gives integer value

b = wing length = 4.61m and

C_{avg}= chord length = 0.566m

Then,

$N_{rib} \approx 9$

Therefore, we need 9 ribs.

For initial design the thickness of ribs is taken as 6mm.

4.5.2. Spar

Two spars are used in design, i.e., Main Spar and Aft Spar. The main spar is taken to be I-beam of 2x3 inch and thickness of 4mm. Similarly, aft spar of thickness 2mm is taken. Changes will be made further as per need of the design.

4.5.3. Aircraft Material

The most popular material for aircraft is Aluminum 2024-T3 due to its ability to resist corrosion, cost effective and appearance, so we have used it for our analysis. (Aircraft and Aerospace Applications: Part One, 2004)

4.5.4. 3D Model of Wing

A 3D model of the wing structure is created using SOLIDWORKS. This is only the initial model, which will be revisited and modified as we carry on the simulation. The summary of initial wing dimension and configuration are as follows:

Table 4.10: Calculated wing design parameters

Wing span (b)	4.61 m
Wing Area (S)	2.61 m^2
Aspect Ratio	8.14
Dihedral	0°
Wing skin thickness	1 mm
No. of ribs	9
Main spar dimensions (mm)	67.45×50×4
Aft Spar dimensions (mm)	23.6×14×2

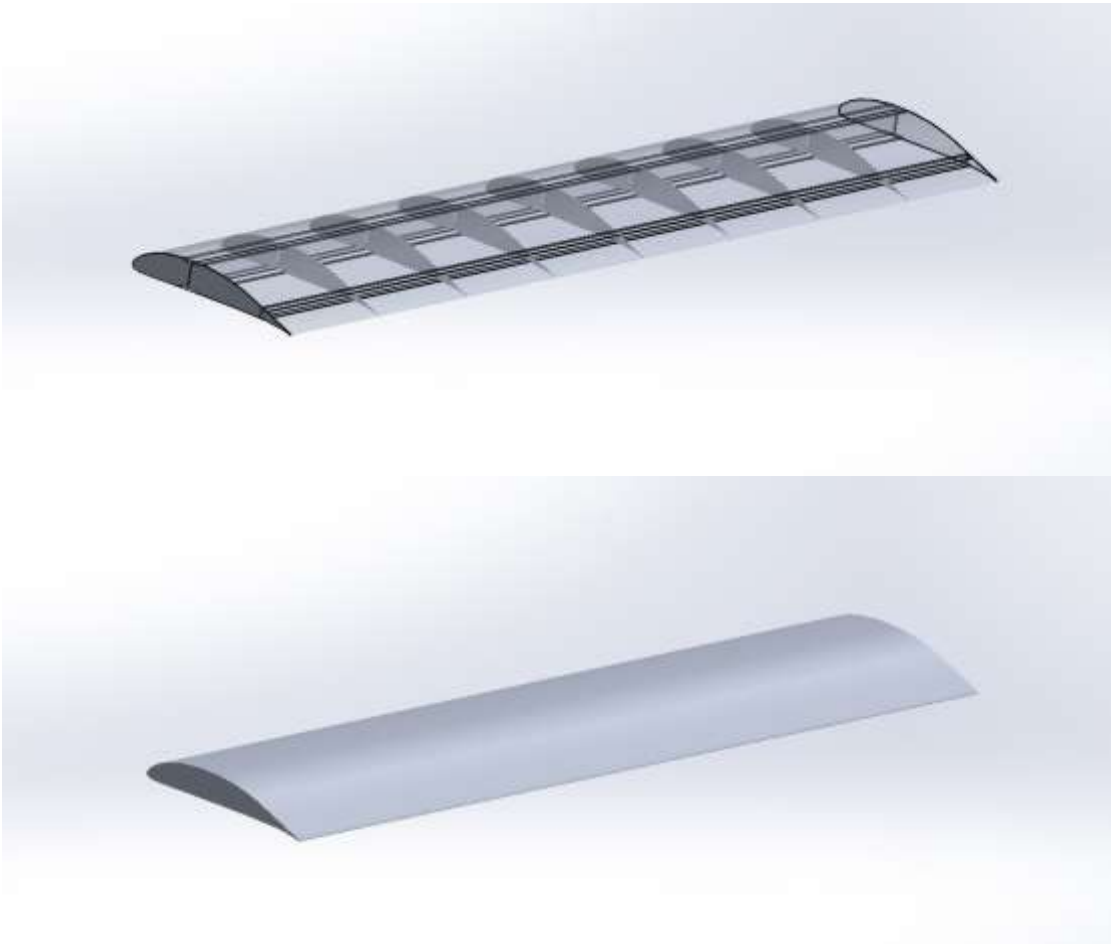

Figure 4.6: CAD model of wing structure designed using SOLIDWORKS

4.6. Fluid Structure Interaction Analysis

After refining the mesh and defining appropriate setups, we ran the Fluent solver. The solution converged after 42 iterations. The residuals had low enough value to indicate good convergence.

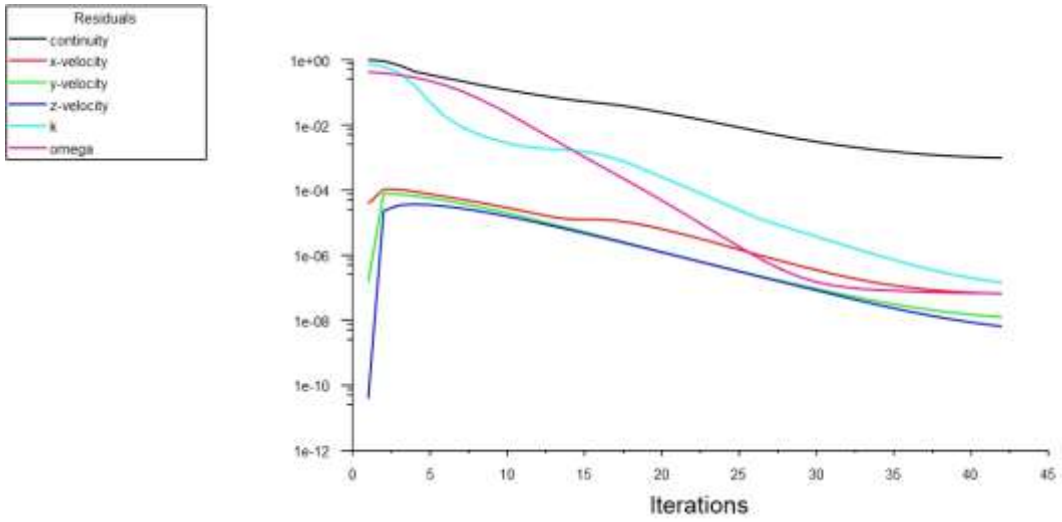

Figure 4.8: Residual graph for fluent solution

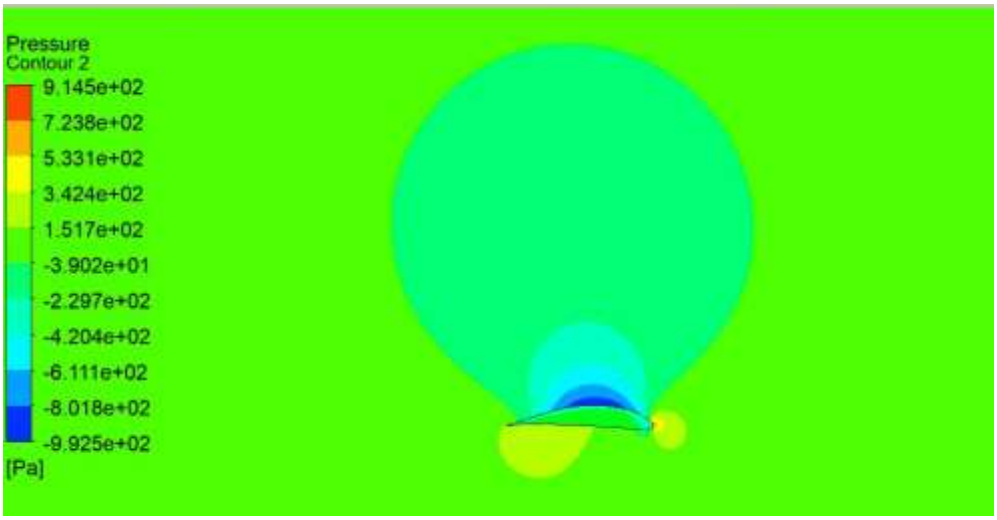

Figure 4.7: Pressure Contour over the wing surface

The pressure is concentrated at the leading edge of the wing as the flowing air strikes it. As the flow progresses over the wing, the pressure at both surface drops. Due to the curvature of wing, the velocity on upper surface increases creating a low-pressure region. High pressure region is generated at the wing trailing edge of the bottom surface of the wing due to decrease in velocity of the air particles at lower surface. This generates the net upward force which creates a lift on the wing. A maximum velocity of 55.43 m/s is observed above the upper surface of wing and a negative gauge pressure of 992.5 Pa is observed at the region.

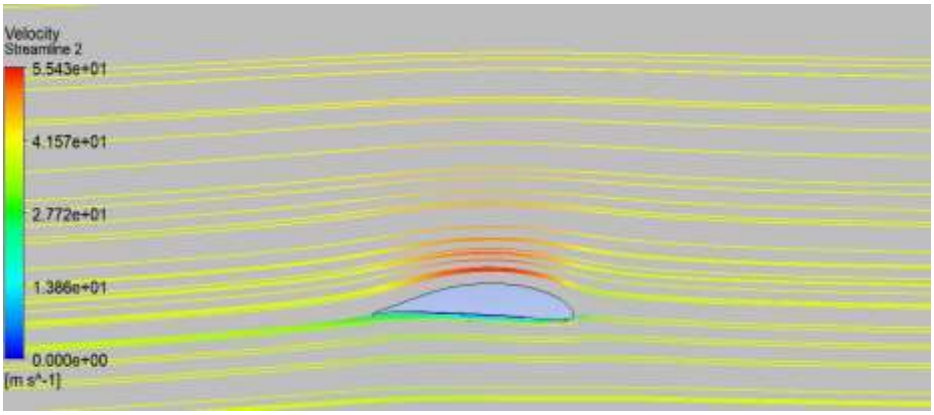

Figure 4.9: Velocity streamline plot

These pressure loads are exported to the structural module and acts as external force on wing structure. The effects of these forces on the wing structure are analyzed using structural simulation.

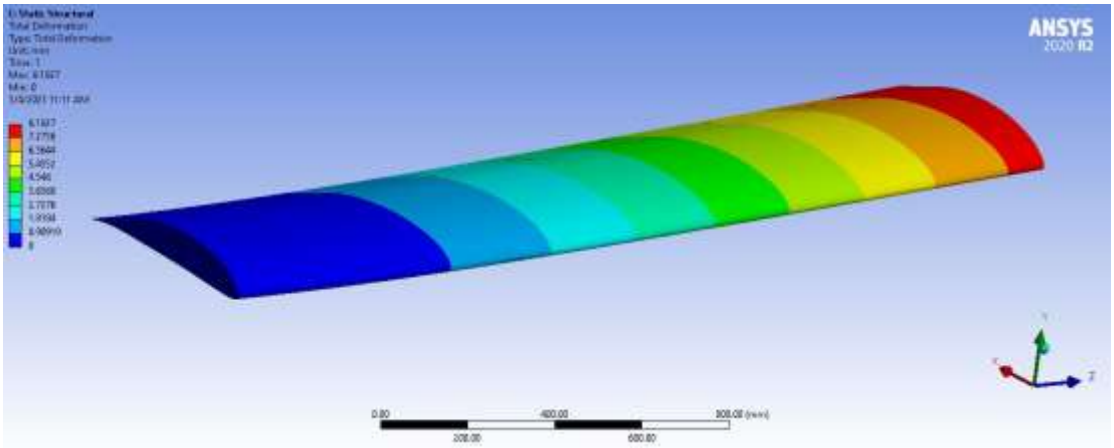

Figure 4.10: Total deformation of wing structure

As the lift forces act on the wing due to pressure gradient over wing surface, certain deformation is created. As the root of the wing is attached to the fuselage, there is no deformation at the root but as it progresses towards the tip, The deformation goes on increasing gradually. The maximum deformation was found to be 8.18 mm at the tip.

Since, the root of the wing is attached to the fuselage, both the bending moment and shear force are higher at this region. The lift generated by wing is distributed along the wingspan but it is concentrated towards the center of the wing, thereby imparting higher load at the root. This causes higher stress at the regions of wing near the root. Maximum

stress observed is 45.06 MPa, which is significantly less than yield strength of the material used for wing, i.e. Aluminum 2024-T3.

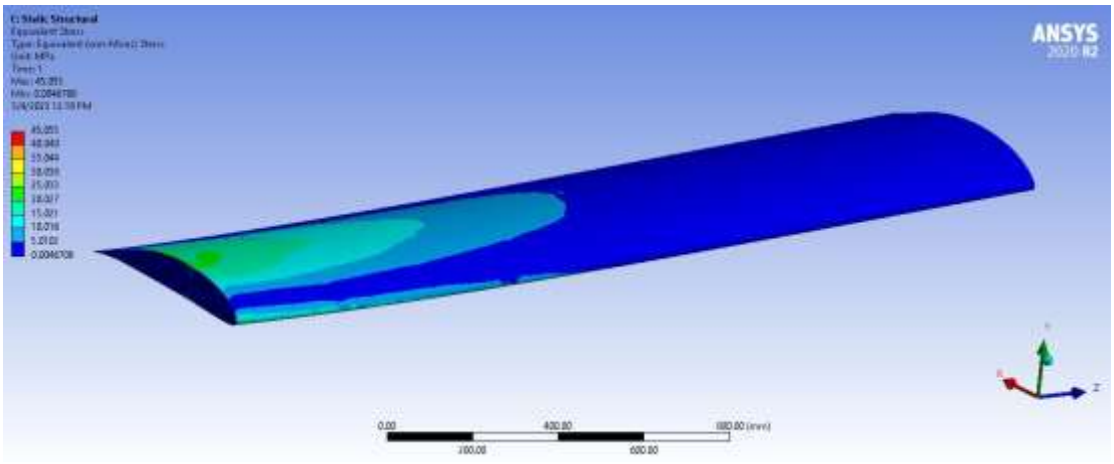

Figure 4.11: Equivalent (Von Mises) stress plot

These overall features show that the design of the wing is suitable for the UAV.

4.7. Comparison of Results

The results obtained from different wing configurations obtained varying wing span, chord length and dihedral angle are compared in the table 4.10. The shaded region represents the condition not safe for operation as the lift factor of safety is less than 1.5.

Table 4.11: FSI simulation results of different wing configurations

S.N.	Aspect Ratio	Wingspan (b) m	Chord length (c) mm	Weight kg	Dihedral (Γ)	Lift (L) N	L/D		Max. Stress (MPa)	Max. Strain (10^4)	Lift factor of safety
							FSI	XFLR5			
1	6	3.96	566	11.89	0	898.85	24.79	22.77	79.01	12.2	1.50
2					1	877.87	20.75	22.77	77.68	12	1.47
3					2	876.74	20.94	22.77	77.863	12.1	1.47
4		4.61	768	18.16	0	1248.75	21.81	21.38	35.81	0.399	2.09
5					1	1555.2	22.64	21.38	34.27	0.376	2.6
6					2	1584.58	22.73	21.38	37.56	0.42	2.64
7	8.14 (original)	4.61	566	13.95	0	1055.4	23.03	24.95	45.055	4.6	1.76
8					1	1073.01	23.05	24.95	36.62	4.7	1.8
9					2	1081.96	23.17	24.95	47.11	8.7	1.81
10	10	4.61	461	11.52	0	839.03	22.73	27.63	48.728	5.42	1.4
11					1	818.45	22.57	27.63	34.806	4.13	1.36
12					2	829.8	22.46	27.63	34.861	4.22	1.39
13		5.11	566	15.45	0	1189.71	23.78	26.54	68.39	8.1	1.99
14					1	1188.6	24.16	26.54	58.67	6.14	1.99
15					2	1202.35	23.98	26.54	65.38	6.51	2.01

4.7.1. Analysis of Mean (ANOM)

First of all, the mean value of L/D obtained from FSI was calculated for each design point. There are 3 design points each for wing parameters: dihedral, wingspan and chord length, This gives general idea on how lift to darg ratios changes with the change in these parameters.

Table 4.12: Mean value of L/D for different design points

Design Point	Dihedral (Γ)	Avg. L/D	Wingspan (b) m	Avg. L/D	Chord length (c) mm	Avg. L/D
1	0°	23.23	3.96	22.16	768	22.40
2	1°	22.59	4.61	23.08	566	23.08
3	2°	22.66	5.11	23.97	461	22.52

Overall mean L/D = (23.23+22.59+22.66+22.16+23.08+23.97+22.40+23.08+22.52)/9

= 22.85

From the calculated data, we generated a ANOM chart for the objective function L/D.

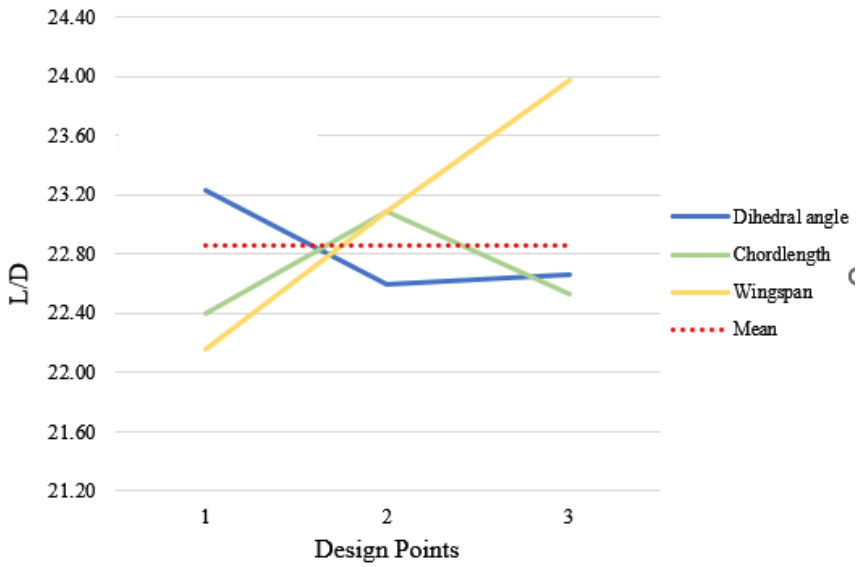

Figure 4.12: ANOM results for the objective function (L/D)

From the results of ANOM, we find out that there is no significant changes in value of L/D, with the change in dihedral angle and chord length. The values of objective function L/D is within 5% mean limits in case of both dihedral and chord length. But the design point 3 for wingspan exceeds the 5% limit, which means there is some significant change in the value of L/D at that design point, i.e., b=5.11m. So, wingspan

is a design factor which has more influence on lift to drag ratio of the wing than dihedral and chord length.

From table 4.10, the maximum value of L/D is 24.16 at b = 5.11 m, c = 566 mm and $\Gamma = 1°$.

Comparing with original design parameter, i.e., b = 4.61m, c = 566mm and $\Gamma = 0°$,

Increase in L/D = (24.16-23.03)/23.03 = 4.9%

CHAPTER FIVE: CONCLUSION AND RECOMMENDATION

5.1. Conclusion

The gross takeoff weight for the intended fixed wing UAV was estimated to be 122 kgs through iterative calculation. The high wing configuration and constant chord planform were selected after analyzing pros and cons of different wing configurations. Using airfoil tools, Wortmann FX 76-MP-140 was selected after comparing various airfoils and analyzing their characteristics curves. Using scaling laws, the required wingspan, wing area and chord of the wing was calculated to be 4.61 meters, 2.61 sq. m and 566 mm respectively. A 3D model of the wing was created using SOLIDWORKS including 9 ribs, I shaped main spar and C shaped aft spar. The designed model was validated using XFLR5 and FSI simulation, which showed acceptable levels of stress, deformation and lift to drag ratios.

Results from 15 different FSI simulations carried out by varying dihedral angle, chord and wingspan, were tabulated and compared with the intent of maximizing the lift to drag ratio (L/D). The designs for wingspan of 3.96 m and designs for the chord length of 461mm were found to be inappropriate as their lift factor of safety were less than 1.5. Using ANOM with 5% mean limits, we found out that dihedral and chord length did not have significant impact on the L/D but wingspan had some significant impact. If the wingspan is changed from 4.61 meters to 5.11 meters and dihedral from 0° to 1° from the original design, the L/D will increase by 4.9%.

5.2. Recommendation

. For better analysis of the wing and its structure, we recommend the following:

- Carry out two-way FSI: The effect of pressure load due to fluid on wing structure was analyzed but the effect of deformation of wing structure on the fluid flow was not studied. By fully coupling the CFD and structural modules, we can get more realistic results.
- Consider the effect of different flight conditions: To evaluate the impact of different flight conditions on the wing structure, we recommend performing FSI analysis for a range of altitude, speed, and angle of attack. This can help identify

the most critical flight conditions and the potential failure modes associated with them.

- Include flaps and ailerons: This will provide more practical insight as they are included in the final design.

REFERENCES

Aircraft and Aerospace Applications: Part One. (2004, March). Retrieved from Total Materia Web site: http://www.totalmateria.com/Article95.htm

Airfoil Tools. (2022). Retrieved from Airfoil Tools: http://airfoiltools.com/

Anggraeni, D., Hidayat, D., Pramutadi, A., & Soemaryanto, A. (2015). Design and Flight Test of a Medium Range UAV for Aerial Photography. *International Journal of Unmanned Systems Engineering*. doi:DOI: 10.14323/ijuseng.2015.12

Center for Accelerating Innovation and Impact. (2018). *UAVs in Global HealthDefining a Collective Path Forward.* Chicago: USAID.

Dahal, C., Dura, H., & Poudel, L. (2021). Design and Analysis of Propeller for High-Altitude Search and Rescue Unmanned Aerial Vehicle. *International Journal of Aerospace Engineering*. doi:https://doi.org/10.1155/2021/6629489

Dalamagkidis, K., Valavanis, K. P., & Piegl, L. (2012). *On Integrating Unmanned Aircraft Systems into the National Airspace System.* Dodrecht: Springer.

Ducard, G., & Allenspach, M. (2021). Review of Designs and Flight Control Techniques of Hybrid and Convertible VTOL UAVs. *Aerospace Science and Technology*. doi:https://doi.org/10.1016/j.ast.2021.107035

Ezkurra, M., Esnaola, J., Martinez-Agirre, M., Extxerberria, U., Lertxundi, U., Colomo, L., Zurutuza, I. (2018). International Journal of Mechanical and Materials Engineering. *Analysis of One-Way and Two-Way FSI Approaches to Characterise the Flow Regime and the Mechanical Behaviour during Closing Manoeuvring Operation of Behaviour during Closing Manoeuvring Operation of a Butterfly Valve*.

Goetzendorf-Grabowski, T., Tarnowski, A., Figat, M., Mieloszyk, J., & Hernik, B. (2020). Lightweight unmanned aerial vehicle for emergency medical service – Synthesis of the layout. *Journal of Aerospace Engineering*.

Gryte, K., Hann, R., Alam, M., Roháč, J., Johansen, T., & Fossen, T. (2018). Aerodynamic Modeling of the Skywalker X8 Fixed-Wing Unmanned Aerial Vehicle. *Iternational Conference on Unmanned Aircraft Systems.* Dallas: IEEE.

Gudmundsson, S. (2014). *General Aviation Aircraft Design: Applied Methods and Procedures.*

Houghton, E. L., & Carpenter, P. W. (2003). *Aerodynamics for Engineering Students.* Burlington: Butterworth-Heinermann.

Iamnepal. (2020, October 30). *home*. Retrieved from Iamnepal: https://iamnepal.co/drots-nepal-medical-drone-of-nepal/

Liu, T. (2006). Comparative Scaling of Flapping- and Fixed-Wing Flyers. *AIAA Journal*, 24-33.

Maughmer, M., & Somerst, D. (1987, Februaury). Design and Experimental Results for a High-Altitude, Long-Endurance Airfoil.

Mazhar, F., & Khan, A. (2010). STRUCTURAL DESIGN OF A UAV WING USING FINITE ELEMENT METHOD. *51st AIAA/ASME/ASCE/AHS/ASC Structures, Structural Dynamics, and Materials Conference.* Orlando, Florida.

McMasters, J., & Henderson, M. (n.d.). LOW-SPEED SINGLE-ELEMENT AIRFOIL SYNTHESIS. *CORE*, 1-31.

Muñoz, J., & Tilvaldyev, S. (2017). Analysis of the Propulsive System for an Unmanned Aerial Vehicle. *International October Conference on Mining and Metallurgy.* Bor Lake: University of Belgrade.

Panagiotou, P., Kaparos, P., & Yakinthos, K. (2014). Winglet design and optimization for a MALE UAV using CFD. *Elsevier*, 190-205.

Panagiotou, P., Kaparos, P., Salpingidou, C., & Yakinthos, K. (2016). Aerodynamic design of a MALE UAV. *Aerospace Science and Technology*.

Pavithran, R., Lalith, V., Naveen, C., Sabari, S., MST, A., & Hariprasad, V. (2020). A Prototype of Fixed Wing UAV for Delivery of Medical Supplies. *IOP Conference Series: Material Science and Engineering.* IOP Publishing. doi:doi:10.1088/1757-899X/995/1/012015

Poole, D., Allen, C., & Rendall, T. C. (2015). Metric-Based Mathematical Derivation of Efficient. *AIAA.* doi:DOI: 10.2514/1.J053427

Prisacariu, V. (2017). The History and the Evolution of UAVs From the Beginning till the 70s. *Journal of Defense Resources Management, 8*(1 (14)), 181-189.

Raymer, D. P. (2018). *Aircraft Design: A Conceptual Approach.* Reston, Virginia: American Institute of Aeronautics and Astronautics, Inc.

Rosheim, M. (2006). *Leonardo's Lost Robots.* Dodrecht: Springer.

Sadraey, M. H. (2013). *Aircraft Design: A Systems Engineering Approach.* Chichester, UK: John Wiley & Sons Ltd.

Sharma, G. (2018, April 30). *Article*. Retrieved from Reuters: https://www.reuters.com/article/nepal-health-drones-idUSL3N1S24S6

Shrestha, A. (2018, March 31). *News*. Retrieved from Techlekh: https://techlekh.com/mahabir-pun-medi-copters/

Sobester, A., Keane, A. J., Scanlan, J., & Bressloff, N. W. (2005). Conceptual Design of UAV Airframes Using a Generic Geometry Service. *American Institute of Aeronautics and Astronautics*.

Sobieczky, H., & Seebas, A. (1984, January). Supercritical Airfoil and Wing Design. *Annual Review of Fluid Mechanics*, pp. 337-363. doi:https://doi.org/10.1146/annurev.fl.16.010184.002005

Sweta. (n.d.). *Aeronautical*. Retrieved from Learnpick: www.learnpick.in

TURANOĞUZ, E. (2015). *Design of a Medium Range Tactical.* Middle East Technical University, Department of Aerospace Engineering. Ankara: Aselsan Inc.

Tyan, M., Nguyen, N. V., Lee, J.-W., & Kim, S. (2016). A Hybrid VTOL-Fixed Wing Electric UAV Sizing Methodology Development. *KSAS 2016 Fall Conference.*

Valavanis, K. P. (2007). *Advances in Unmanned Aerial Vehicles.* (K. P. Valavanis, Ed.) Dordrecht, Netherlands: Springer.

Zong, J., Zhu, B., Hou, Z., Yang, X., & Zhai, J. (2021). Evaluation and Comparison of Hybrid Wing VTOL UAV with Four Different Electric Propulsion Systems. *Aerospace*. doi:https://doi.org/10.3390/aerospace8090256

APPENDIX A: PRESSURE CONTOUR PLOT

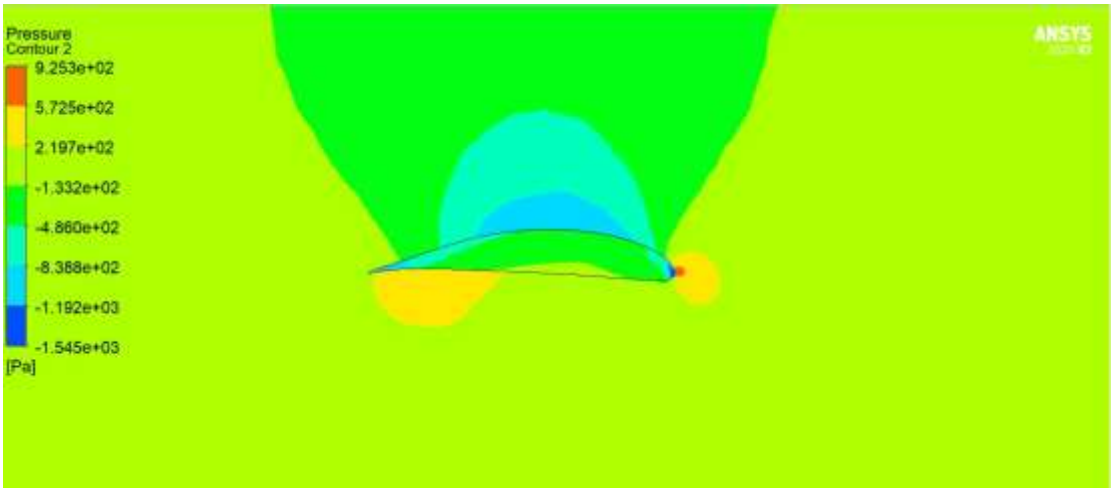

Γ=0°

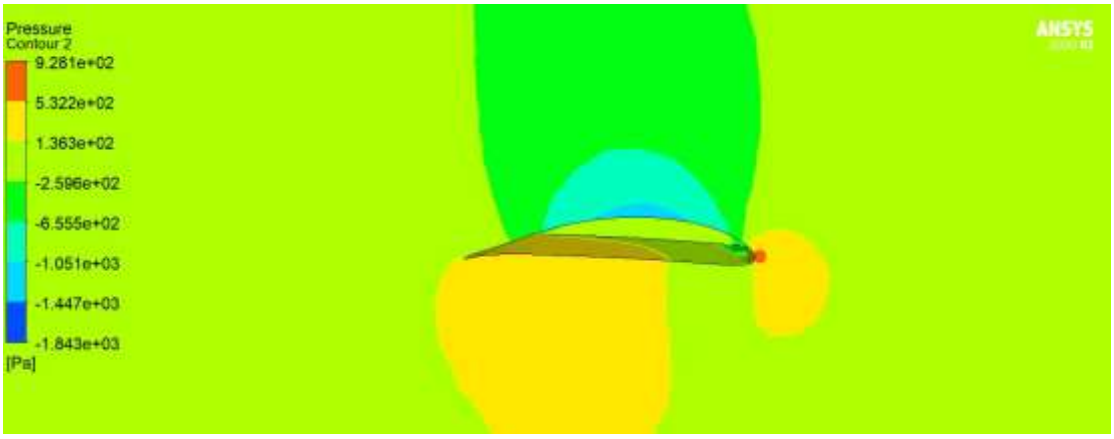

Γ=1°

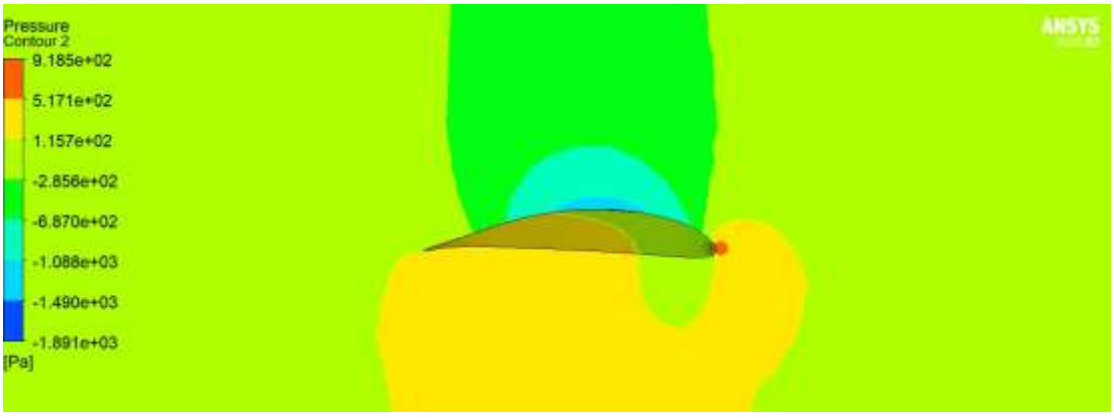

Γ=2°

Figure A.1: Pressure distribution over wing surface having b=4.61m, c=0.566m

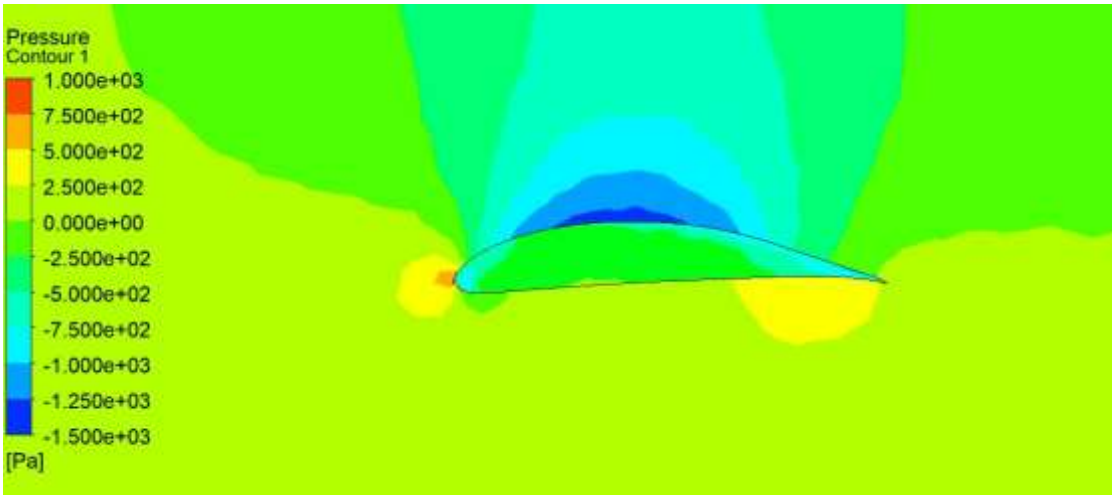

Γ=0°

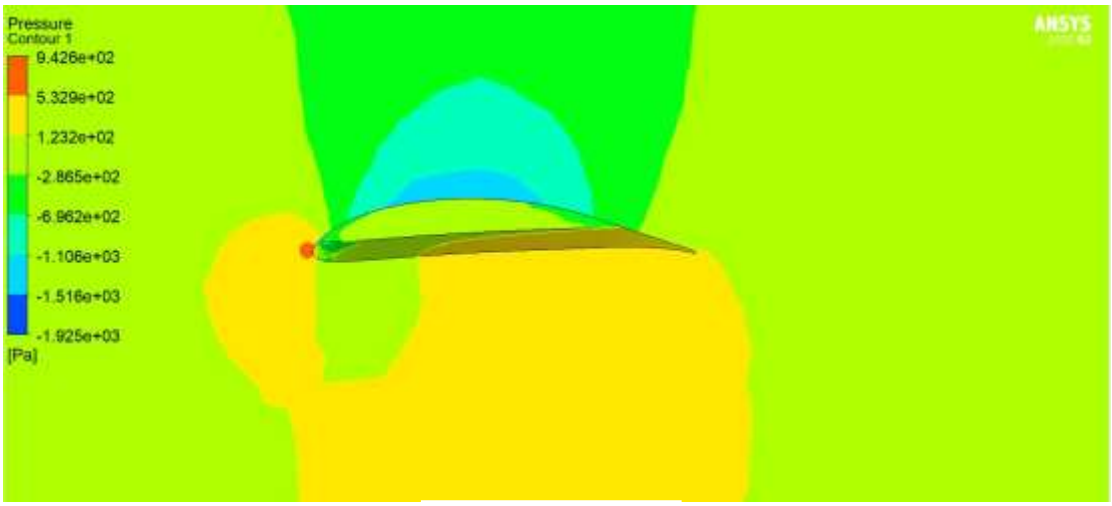

Γ=1°

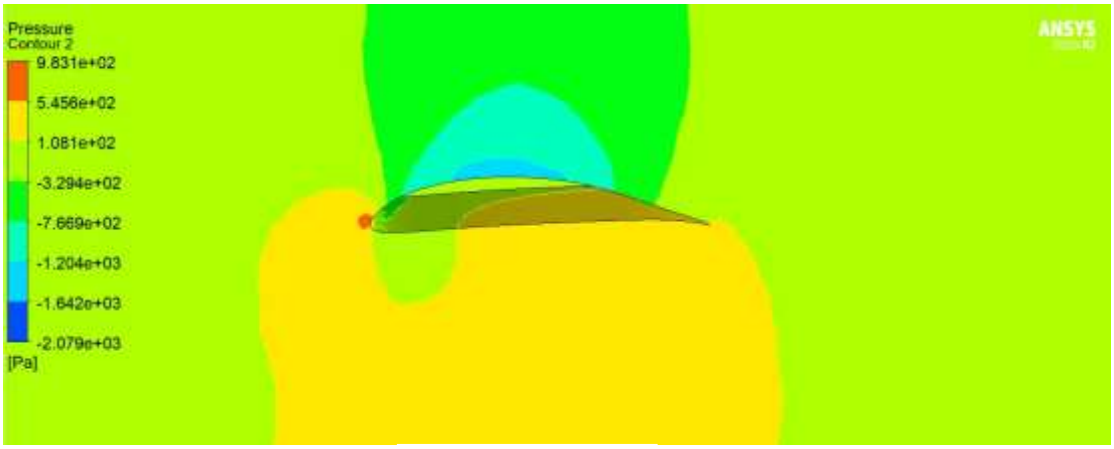

Γ=2°

Figure A.2: Pressure distribution over wing surface having b=4.61m, c=0.768m

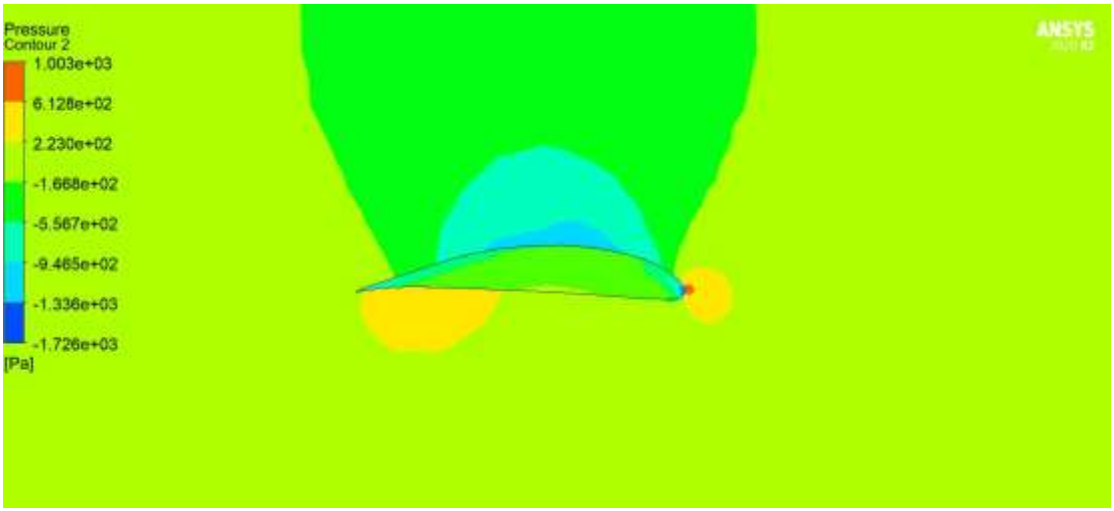

Γ=0°

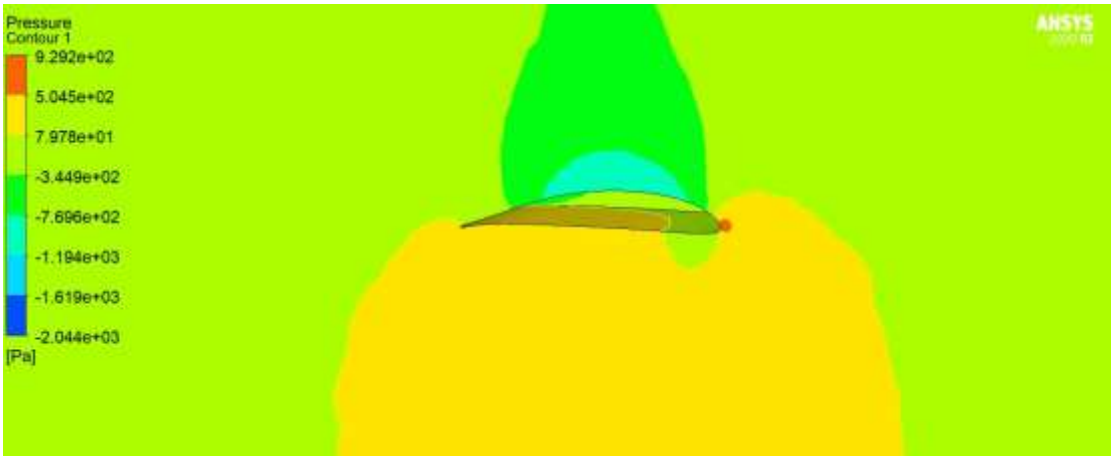

Γ=1°

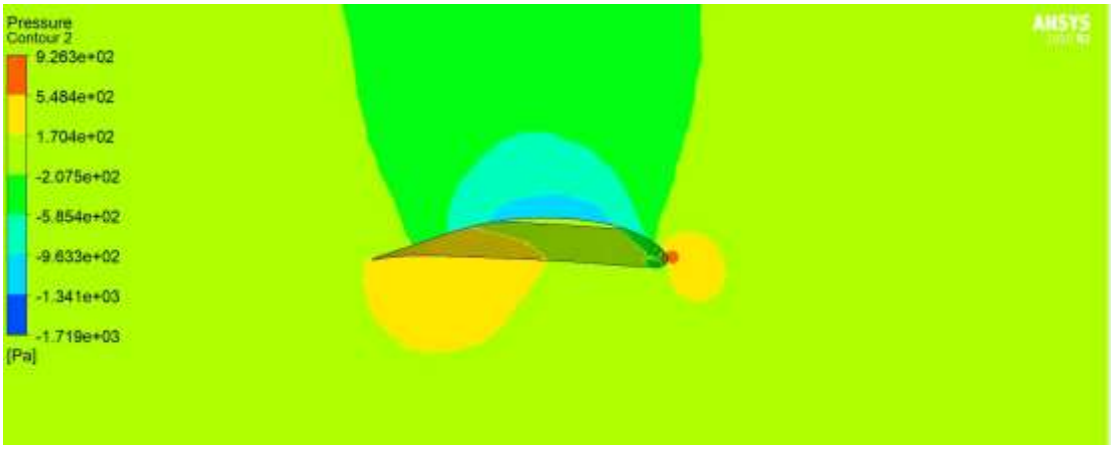

Γ=2°

Figure A.3: Pressure distribution over wing surface of wing having b=3.96m, c=0.566m

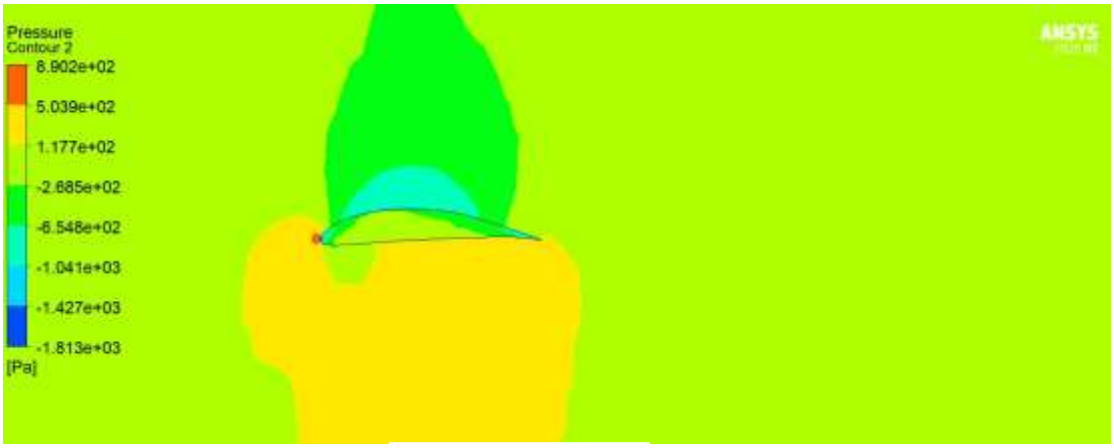

Γ=0°

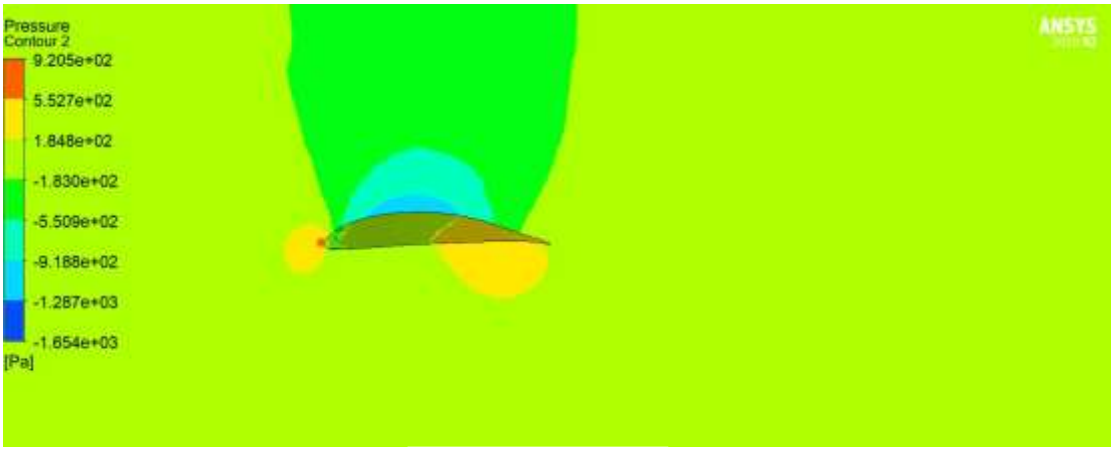

Γ=1°

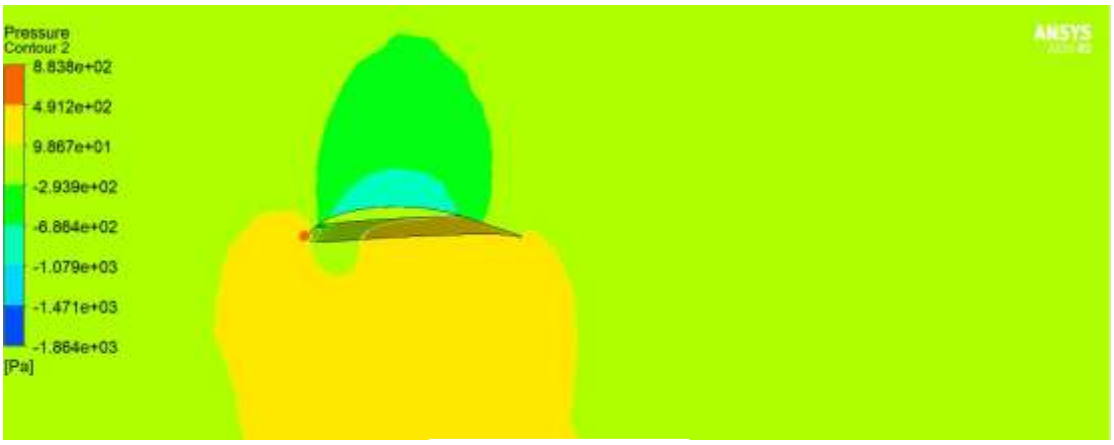

Γ=2°

Figure A.4: Pressure distribution over wing surface of wing having b=4.61m, c=0.461m

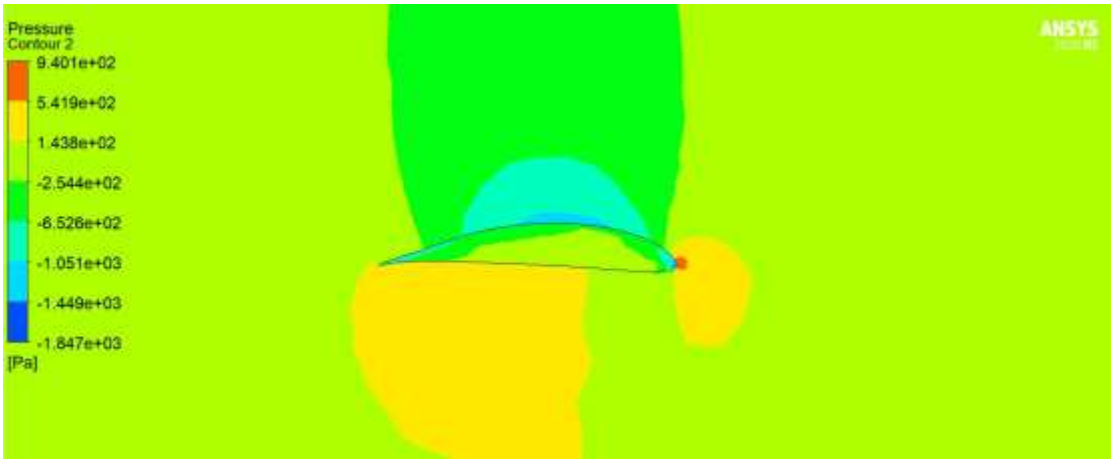

Γ=0°

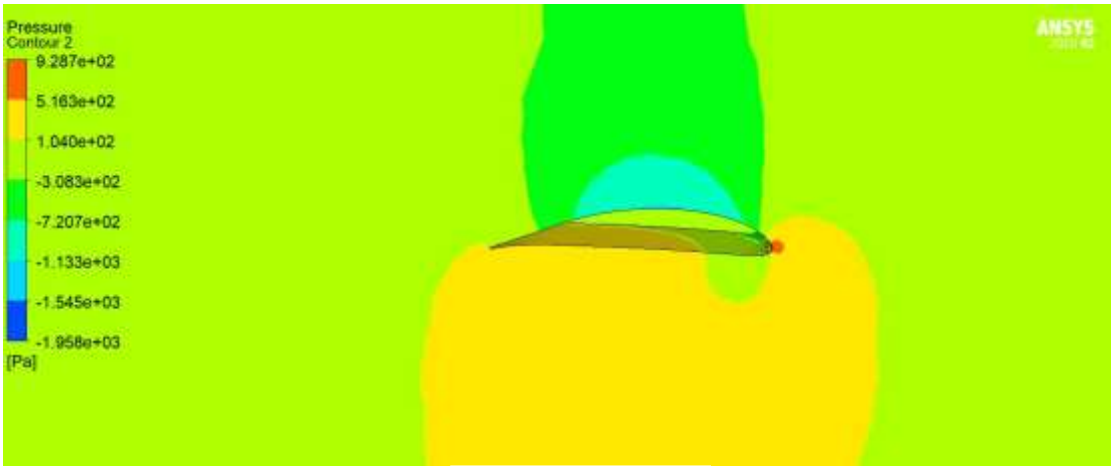

Γ=1°

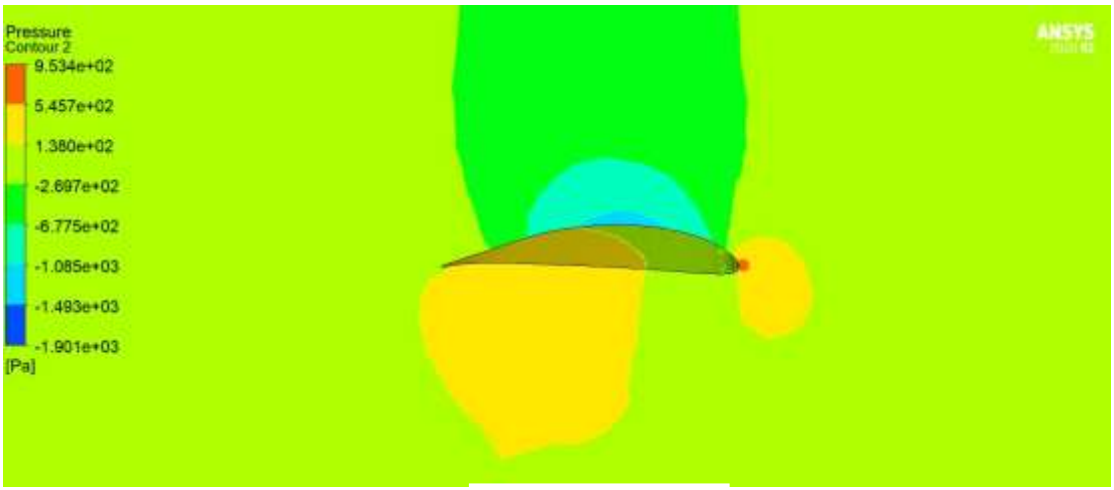

Γ=2°

Figure A.5: Pressure distribution over wing surface of wing having b=5.11m, c=0.566m

APPENDIX B: EQUIVALENT STRESS PLOT

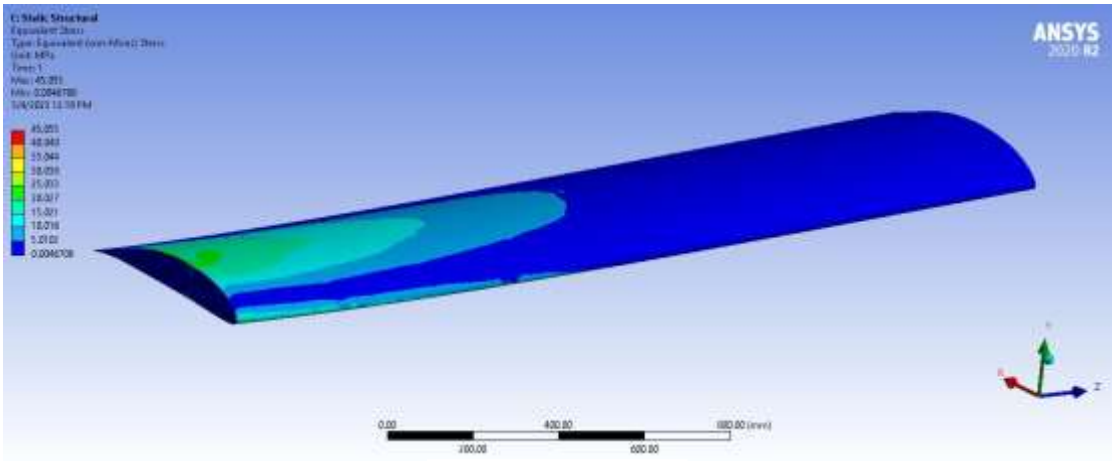

Γ=0°

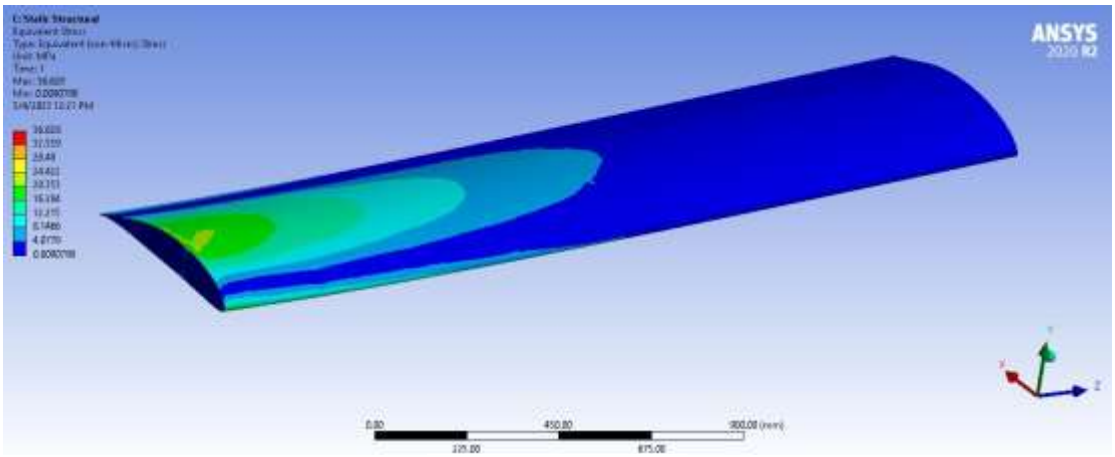

Γ=1°

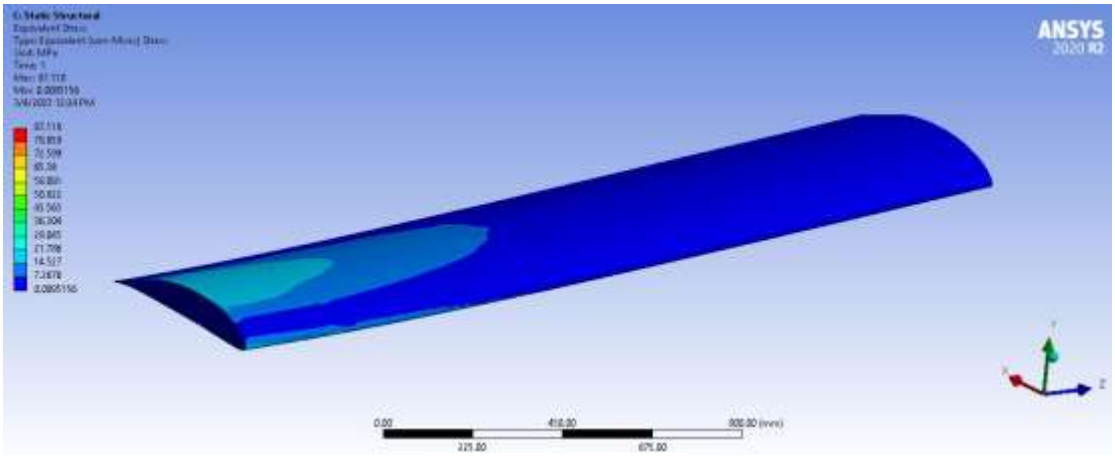

Γ=2°

Figure B.1: Equivalent (Von Mises Stress) Plot of Wings having b=4.61m and c=0.566m

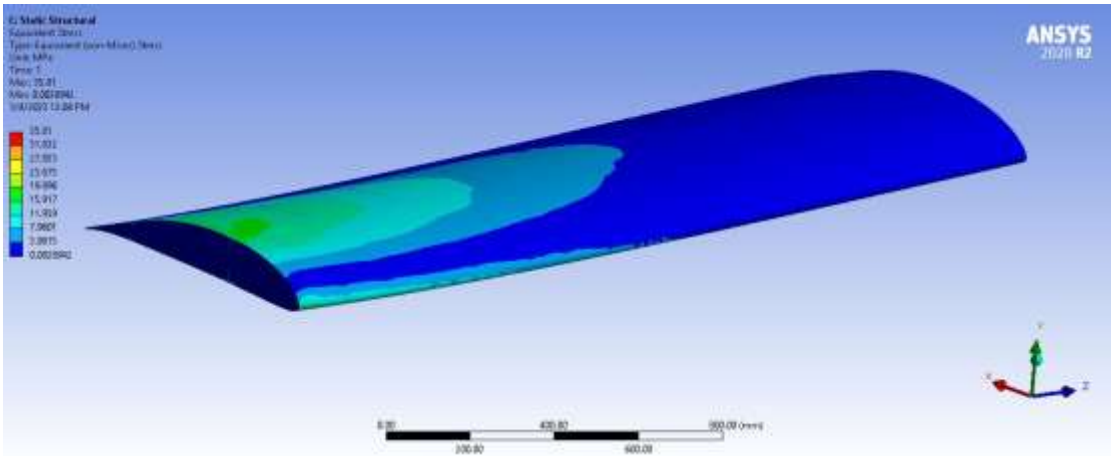

Γ=0°

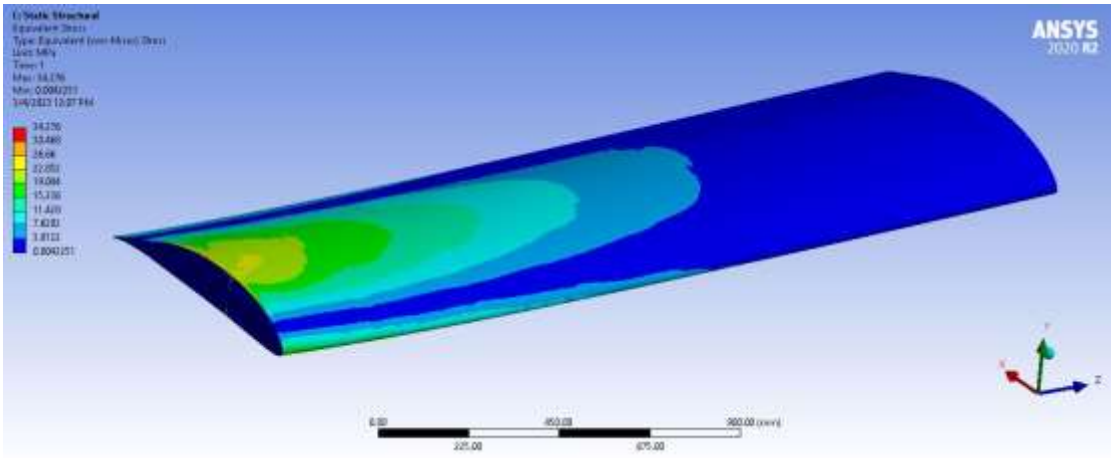

Γ=1°

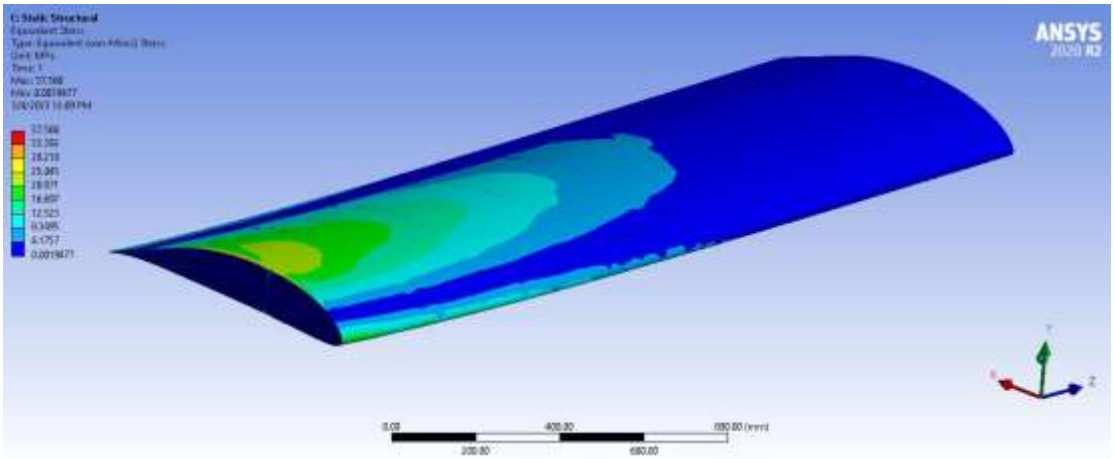

Γ=2°

Figure B.2: Equivalent (Von Mises Stress) Plot of Wings having b=4.61m and c=0.768m

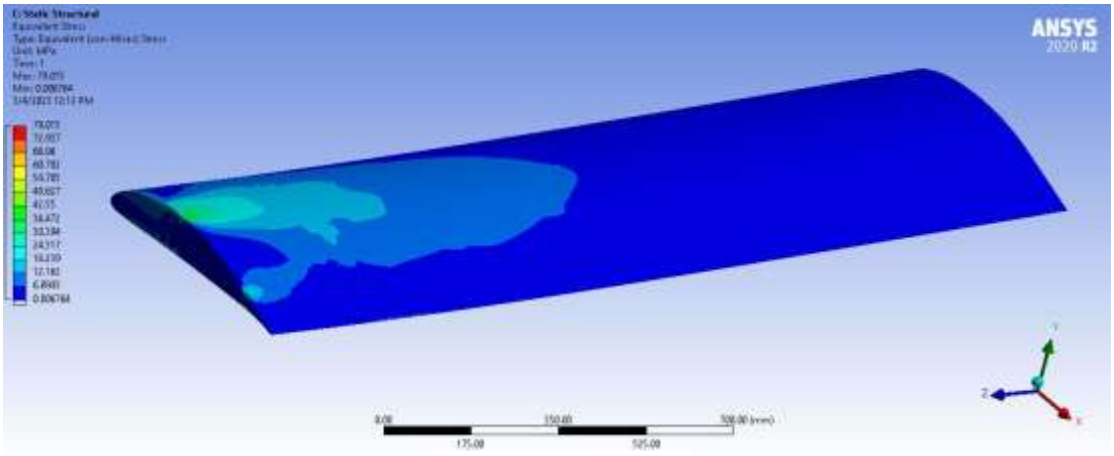

Γ=0°

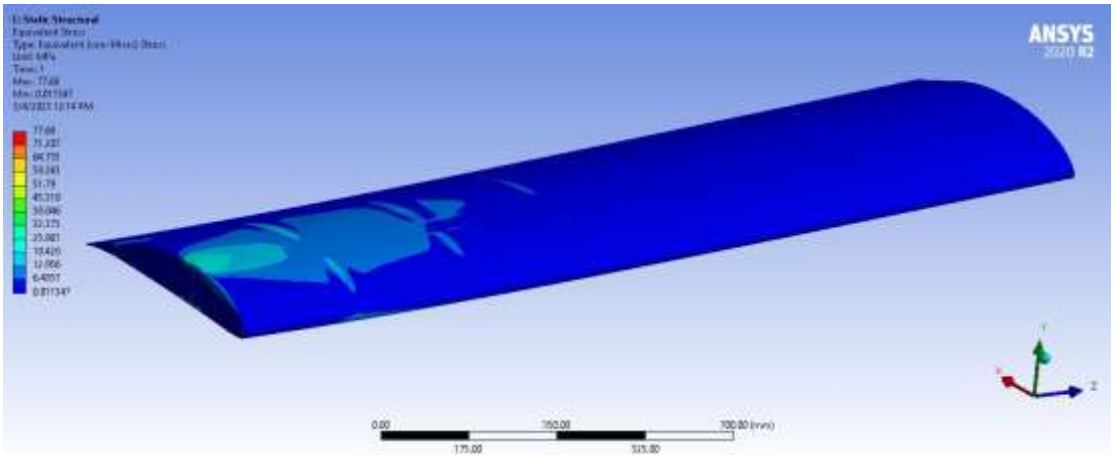

Γ=1°

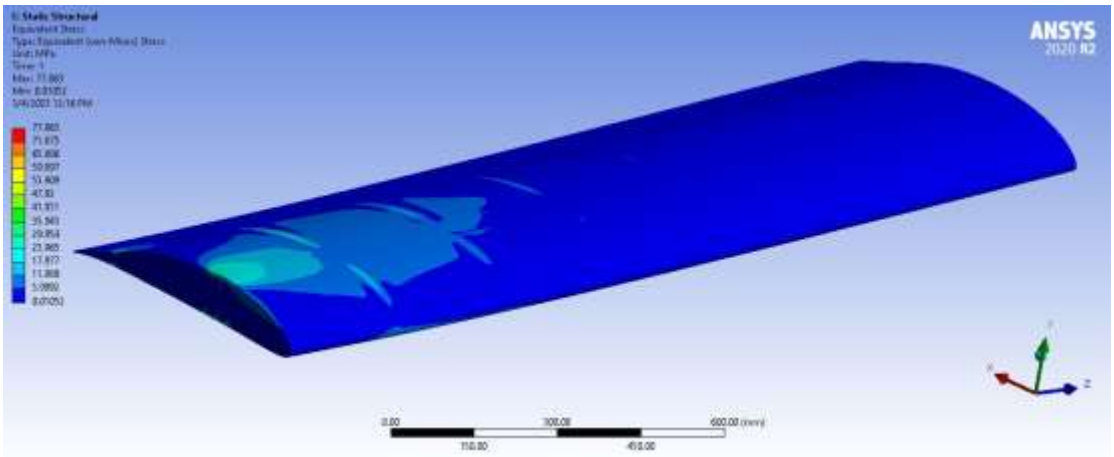

Γ=2°

Figure B.3: Equivalent (Von Mises Stress) Plot of Wings having b=3.96m and c=0.566m

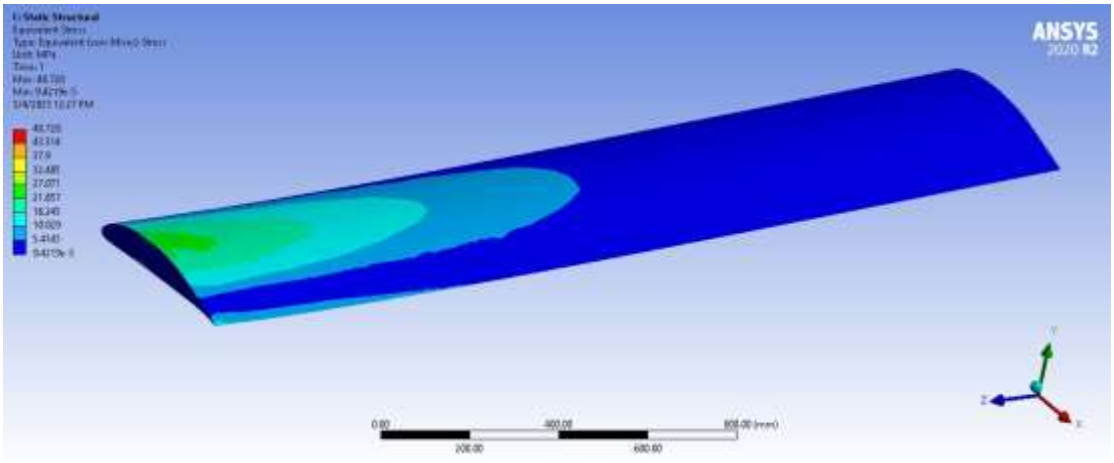

Γ=0°

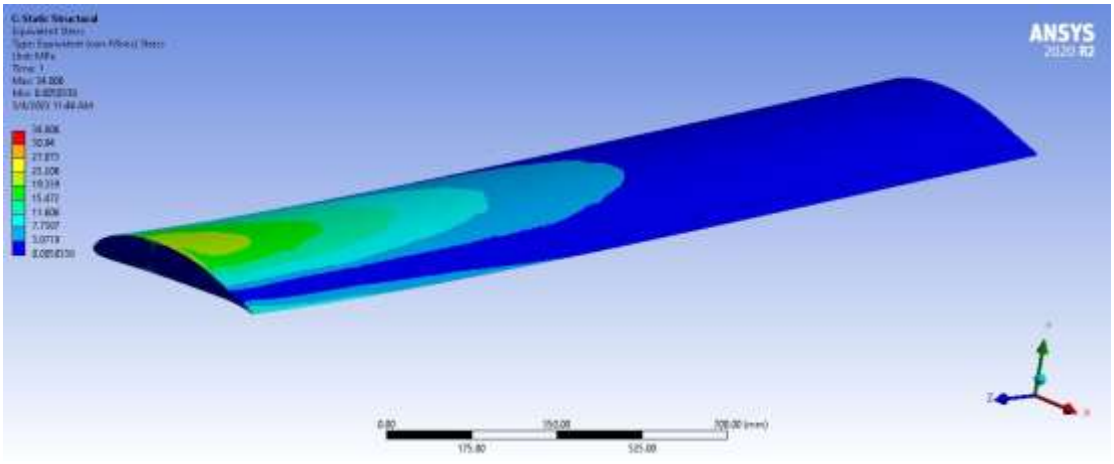

Γ=1°

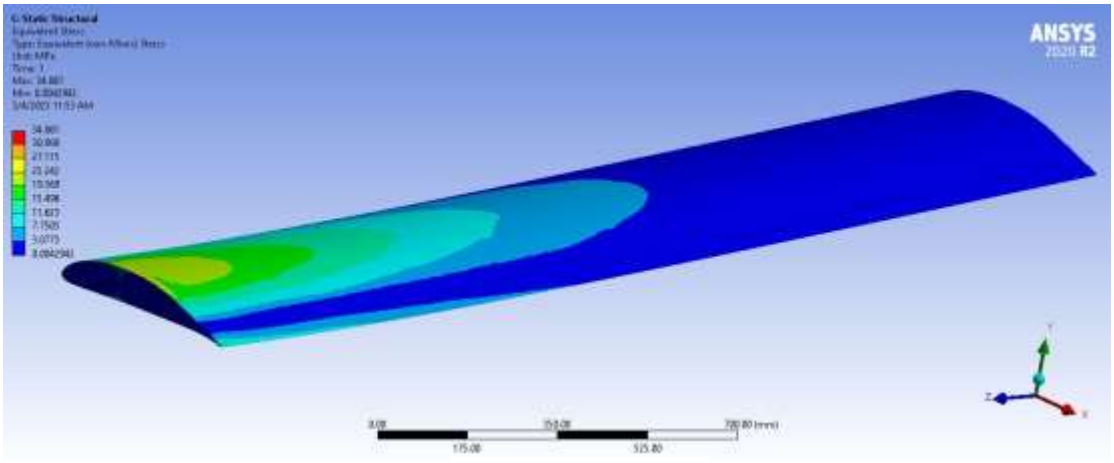

Γ=2°

Figure B.4: Equivalent (Von Mises Stress) Plot of Wings having b=4.61m and c=0.461m

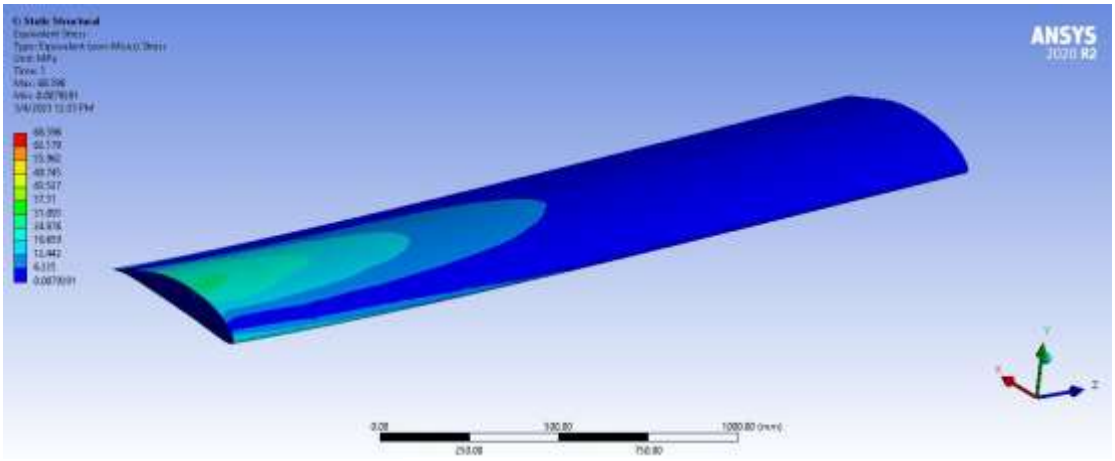

Γ=0°

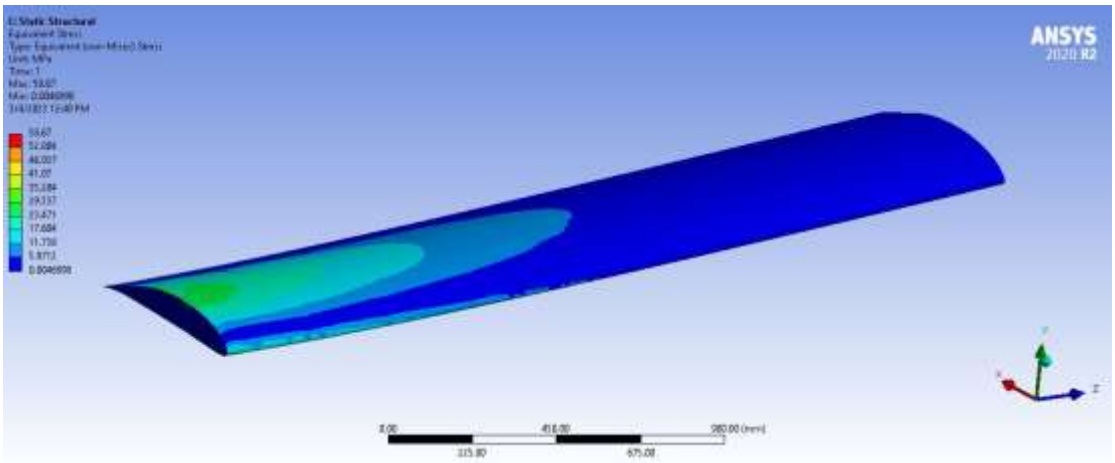

Γ=1°

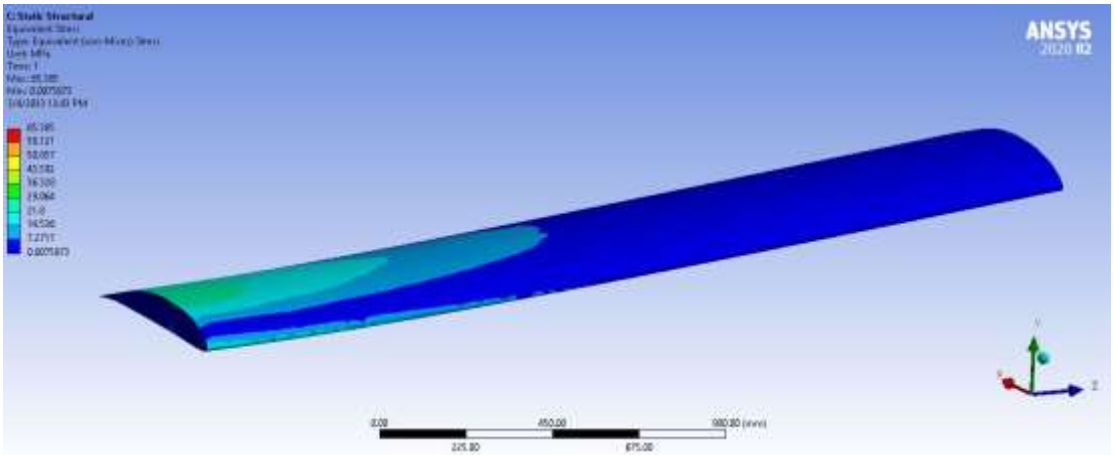

Γ=2°

Figure B.5: Equivalent (Von Mises Stress) Plot of Wings having b=5.11m and c=0.566m

Design And Fluid-Structure Interaction Study of a Wing Structure for a Medium-Range UAV

ORIGINALITY REPORT

17%
SIMILARITY INDEX

PRIMARY SOURCES

1	www.readbag.com Internet	230 words — 2%
2	journal.dresmara.ro Internet	159 words — 2%
3	amslaurea.unibo.it Internet	149 words — 1%
4	mafiadoc.com Internet	134 words — 1%
5	archive.org Internet	113 words — 1%
6	technoplane.hd.free.fr Internet	75 words — 1%
7	journals.pen2print.org Internet	59 words — 1%
8	etd.lib.metu.edu.tr Internet	43 words — < 1%
9	soaneemrana.org Internet	39 words — < 1%